Mycobacterium leprae intracellular survival relies on cholesterol accumulation in infected macrophages: a potential target for new drugs for leprosy treatment

Katherine A. Mattos,[1†] Viviane C. G. Oliveira,[1]
Marcia Berrêdo-Pinho,[1] Julio J. Amaral,[1‡]
Luis Caetano M. Antunes,[2§] Rossana C. N. Melo,[3]
Chyntia C. D. Acosta,[1] Danielle F. Moura,[4]
Roberta Olmo,[4] Jun Han,[5] Patricia S. Rosa,[6]
Patrícia E. Almeida,[3,7] B. Brett Finlay,[2]
Christoph H. Borchers,[5] Euzenir N. Sarno,[4]
Patricia T. Bozza,[7] Georgia C. Atella[8] and
Maria Cristina V. Pessolani[1*]

[1]*Laboratório de Microbiologia Celular, Instituto Oswaldo Cruz, Fundação Oswaldo Cruz, Rio de Janeiro, 21040-900, RJ, Brazil.*

[2]*Michael Smith Laboratories, The University of British Columbia, Vancouver, V6T1Z4, BC, Canada.*

[3]*Laboratório de Biologia Celular, Departamento de Biologia, Universidade Federal de Juiz de Fora, Juiz de Fora, 36036-900, Minas Gerais, Brazil.*

[4]*Laboratório de Hanseníase, Instituto Oswaldo Cruz, Fundação Oswaldo Cruz, Rio de Janeiro, 21040-900, RJ, Brazil.*

[5]*University of Victoria – Genome BC Proteomics Centre, University of Victoria, Victoria, V8Z7X8, BC, Canada.*

[6]*Instituto Lauro de Souza Lima, Bauru,17034-971, SP, Brazil.*

[7]*Laboratório de Imunofarmacologia, Instituto Oswaldo Cruz, Fundação Oswaldo Cruz, Rio de Janeiro, 21040-900, RJ, Brazil.*

[8]*Laboratório de Bioquímica de Lipídeos e Lipoproteínas, Instituto de Bioquímica Médica, Universidade Federal do Rio de Janeiro, Rio de Janeiro, 21940-590, RJ, Brazil.*

Summary

We recently showed that *Mycobacterium leprae* (ML) is able to induce lipid droplet formation in infected macrophages. We herein confirm that cholesterol (Cho) is one of the host lipid molecules that accumulate in ML-infected macrophages and investigate the effects of ML on cellular Cho metabolism responsible for its accumulation. The expression levels of LDL receptors (LDL-R, CD36, SRA-1, SR-B1, and LRP-1) and enzymes involved in Cho biosynthesis were investigated by qRT-PCR and/or Western blot and shown to be higher in lepromatous leprosy (LL) tissues when compared to borderline tuberculoid (BT) lesions. Moreover, higher levels of the active form of the sterol regulatory element-binding protein (SREBP) transcriptional factors, key regulators of the biosynthesis and uptake of cellular Cho, were found in LL skin biopsies. Functional *in vitro* assays confirmed the higher capacity of ML-infected macrophages to synthesize Cho and sequester exogenous LDL-Cho. Notably, Cho colocalized to ML-containing phagosomes, and Cho metabolism impairment, through either *de novo* synthesis inhibition by statins or depletion of exogenous Cho, decreased intracellular bacterial survival. These findings highlight the importance of metabolic integration between the host and bacteria to leprosy pathophysiology, opening new avenues for novel therapeutic strategies to leprosy.

Introduction

Leprosy remains an important cause of morbidity in developing countries, with the detection of approximately 250 000 new cases per annum (WHO, 2011). Also known as Hansen's disease, leprosy manifests as a spectrum of clinical forms that correlate with the nature and magnitude of the innate and adaptive immune responses generated during *Mycobacterium leprae* (ML) infection. In the absence of an appropriate experimental model to study leprosy, the human leprosy lesion has been used for decades in attempts to unravel the complex clinical presentation of the disease. In the early stages of leprosy

research, Ridley and Jopling established a clinical–immunological spectrum of the disease based on the histopathological aspects of the lesions (Ridley and Jopling, 1966). At one extreme, individuals with tuberculoid leprosy (TT) have few lesions, presenting a contained, self-limited infection in which scarce bacilli are detected. On the other end, lepromatous leprosy (LL) is a progressive and disseminated disease characterized by extensive bacterial multiplication within host cells (Scollard *et al.*, 2006).

An important aspect that deserves attention during infection is lipid homeostasis since it is known to play important roles in host–pathogen interactions (Wenk, 2006; van der Meer-Janssen *et al.*, 2010). This also seems to occur in leprosy, which is characterized by collections of heavily infected macrophages with a typically 'foamy' appearance (also referred to as Virchow or Lepra cells) in LL dermal lesions (Virchow, 1863; Scollard *et al.*, 2006). Close examination of these cells revealed that ML resides and replicates within enlarged, lipid-filled phagosomes (Chatterjee *et al.*, 1959), suggesting an important lipid metabolism alteration during infection. Although it was initially believed that these lipids were ML-derived [such as phthiocerol dimycocerosate (PDIM)/dimycocerosate (DIM) and phenolic glycolipid-1(PGL-I)] (Sakurai and Skinsnes, 1970; Kaplan *et al.*, 1983; Brennan, 1984), recent reports have indicated the accumulation of host-derived lipids in these cells (Cruz *et al.*, 2008; Mattos *et al.*, 2010). It has been shown that the Virchow cells found in dermal lesions are highly positive for adipose differentiation-related protein (ADRP), a classical lipid droplet (LD) marker, indicating that their foamy appearance is at least in part derived from the accumulation of LDs (Tanigawa *et al.*, 2008; Mattos *et al.*, 2010). Additionally, it has been shown that ML suppresses lipid degradation through inhibition of hormone-sensitive lipase (HSL) expression, contributing to lipid accumulation in infected macrophages (Tanigawa *et al.*, 2012). Moreover, ADRP has been found to be induced by ML infection and to localize to ML-containing phagosomes in host cells, indicating a close association between LDs and the pathogen-containing vacuole (Tanigawa *et al.*, 2008; Mattos *et al.*, 2011a). More recently, we analysed nerve biopsies and used *in vitro* cultures of Schwann cells to show that the foamy degeneration of the LL nerves are also related to LD biogenesis induced by ML infection and that this process plays a central role in bacterial survival (Mattos *et al.*, 2011a,b).

The intimate dependence of mycobacteria on host lipid molecules for successful infection and persistence has been recently analysed in the context of *Mycobacterium bovis* BCG and *M. tuberculosis* (Mtb). Like ML, BCG and Mtb also mediate foam-cell formation and depend on host lipid acquisition for survival (D'Avila *et al.*, 2006; Pandey and Sassetti, 2008; Almeida *et al.*, 2009; Kim *et al.*, 2010;

Lee *et al.*, 2013). Among these lipids, cholesterol (Cho) turned out to be essential during Mtb infection in that the bacillus is able to degrade and use this lipid molecule as an energy and carbon source for the biosynthesis of mycobacterial lipids (Pandey and Sassetti, 2008). In the case of ML, we also found increased levels of Cho and cholesteryl ester (ChoE) in infected cells (Mattos *et al.*, 2010; 2011a), but the capacity of the leprosy bacillus to metabolize this lipid and its potential role in leprosy pathogenesis remain unclear.

Excess free Cho is toxic to cells, so it is stored as ChoE in LDs. Cellular Cho levels, tightly regulated by a very complex mechanism, result from the balance of three major processes: *de novo* synthesis, internalization of exogenous Cho, and the efflux of excess Cho (van der Wulp *et al.*, 2013). An imbalance in these homeostatic mechanisms can lead to the formation of foam cells, seen in leprosy and tuberculosis, and comparable to the phenotype observed in atherosclerotic lesions (Reiss and Glass, 2006). The present study confirms that Cho is one of the host lipid molecules that accumulate in ML-infected macrophages. We, therefore, investigated the effects of ML on cellular Cho metabolism responsible for its accumulation. By doing so, we found that ML increases Cho *de novo* synthesis and the uptake of exogenous LDL-Cho in the host cell by upregulating the expression of genes involved in these pathways. Moreover, we showed that Cho localized to ML-containing phagosomes and that Cho metabolism impairment significantly decreased intracellular bacterial survival. Our data contribute to the definition of essential host cell pathways exploited by ML during infection that could be used for the rational design of more effective anti-ML therapies.

Results

ML infection alters host lipid composition

In order to study perturbations in host lipid metabolism during ML infection, we analysed the lipid composition of skin biopsy specimens taken from LL and BT patients. Accumulation of lipids as LDs occurs in leprosy skin lesions of LL patients but not of BT patients, as clearly seen by ADRP expression, a marker of LD organelles, through immunohistochemical labelling (Fig. 1A), and qRT-PCR (Fig. 1B). Transcriptional levels of the ADRP gene were 5.7-fold higher in LL patients when compared to BT (BT: 0.89 ± 0.3 and LL: 5.7 ± 1.2, $P = 0.0021$). A quantitative HPTLC analysis of the major neutral lipid species in leprosy biopsies (Fig. 1D, quantification of Fig. 1C) documents a higher enrichment in ChoE (approximately eightfold) when LL samples were compared to BT biopsies. Minor but significant increments in free Cho (approximately twofold) and diacylglycerol (DG, approximately twofold)
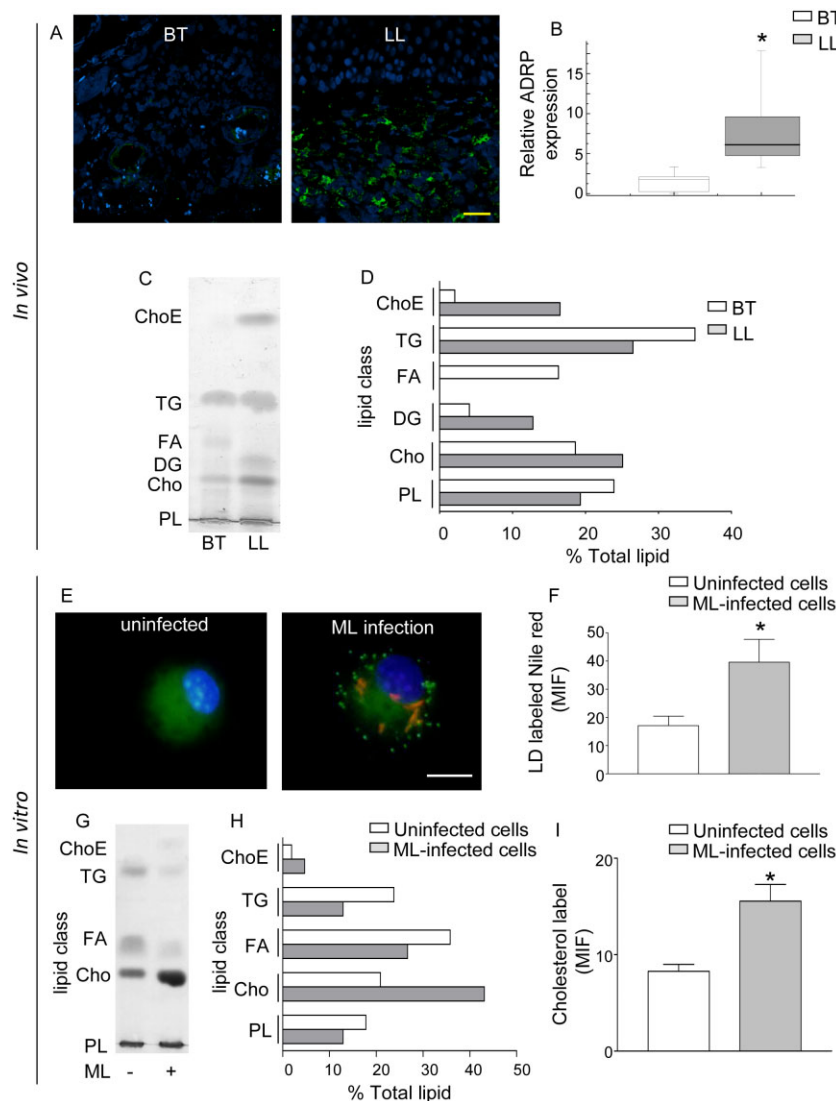
Fig. 1. Lipid accumulation *in vivo* and *in vitro* in ML-infected tissues and cells.
A. Sections of skin biopsies from BT and LL patients (*n* = 4) were immunostained for ADRP and observed by immunofluorescence confocal microscopy. Bar: 20 μm (yellow).
B. Total RNA was extracted from BT and LL biopsies, and expression of ADRP was normalized to GADPH and quantified by qRT-PCR. Values are the average of four independent experiments.
C. Representative HPTLC of neutral lipids extracted from skin biopsies of BT and LL patients detected by charring.
D. The content of each class of lipids was estimated by densitometry and plotted as a percentage.
E. Lipid accumulation in uninfected and ML-infected macrophages was observed by immunostaining for ADRP. Bar: 10 μm (white).
F. LD formation was measured by Nile Red staining.
G and H. (G) Representative HPTLC of neutral lipids extracted from macrophages treated or not with ML and (H) the percentage of each class of lipids estimated by densitometry.
I. Quantitative Cho levels estimated by filipin staining and flow cytometry.
In (A) and (E) Nuclei (blue) were labelled with DAPI. No fluorescence was observed for the Alexa546-labelled mouse isotype control IgG. In HPTLC, the position of pure standard lipids is indicated on the margin of the panel.
*Statistically significant differences ($P \leq 0.05$) comparing LL groups, BT groups, and ML-infected cells versus uninfected cells.

were also observed in LL biopsies in comparison to BT ones. These data suggest that the foamy phenotype of LL lesions is at least in part derived from host Cho accumulation, which could be induced by the chronic and massive presence of ML. *In vitro* assays with human macrophages were then performed to analyse host lipid modulation at early time points during ML infection. In agreement with the biopsy analyses, the presence of ML induced similar lipid sequestration in LD organelles and foam-cell formation in human macrophages infected with ML for 48 h, as shown by ADRP expression using confocal microscopy (Fig. 1E). Alternatively, the LD formation was monitored by flow cytometry, with ML-infected macrophages showing twofold higher values of Mean Fluorescence Intensity (MIF) with Nile red probe in comparison to uninfected cells (Fig. 1F). In addition, the lipid composition of infected cells was analysed by HPTLC in comparison to uninfected cultures (Fig. 1G). A quantita-

tive analysis (Fig. 1H) of a representative HPTLC showed significantly increased levels of free Cho (~ 2-fold) and ChoE (~ 2.5-fold) when compared to uninfected control cultures. Moreover, the Cho cell content was monitored by labelling cells with filipin. As shown in Fig. 1I, ML-infected macrophages showed approximately twofold higher MIF values in comparison to uninfected cells (8.3 ± 0.7 and 15.5 ± 1.7, respectively, $P = 0.0081$). From a physiological point of view, the similar lipid patterns observed *in vitro and in vivo* (early and late infection, respectively) suggest a pathogen-driven host metabolic shift in the Cho pathway.

ML infection induces host *de novo* cholesterol biosynthesis

In order to gain further insights into the effects of ML infection on host lipid metabolism, we performed a
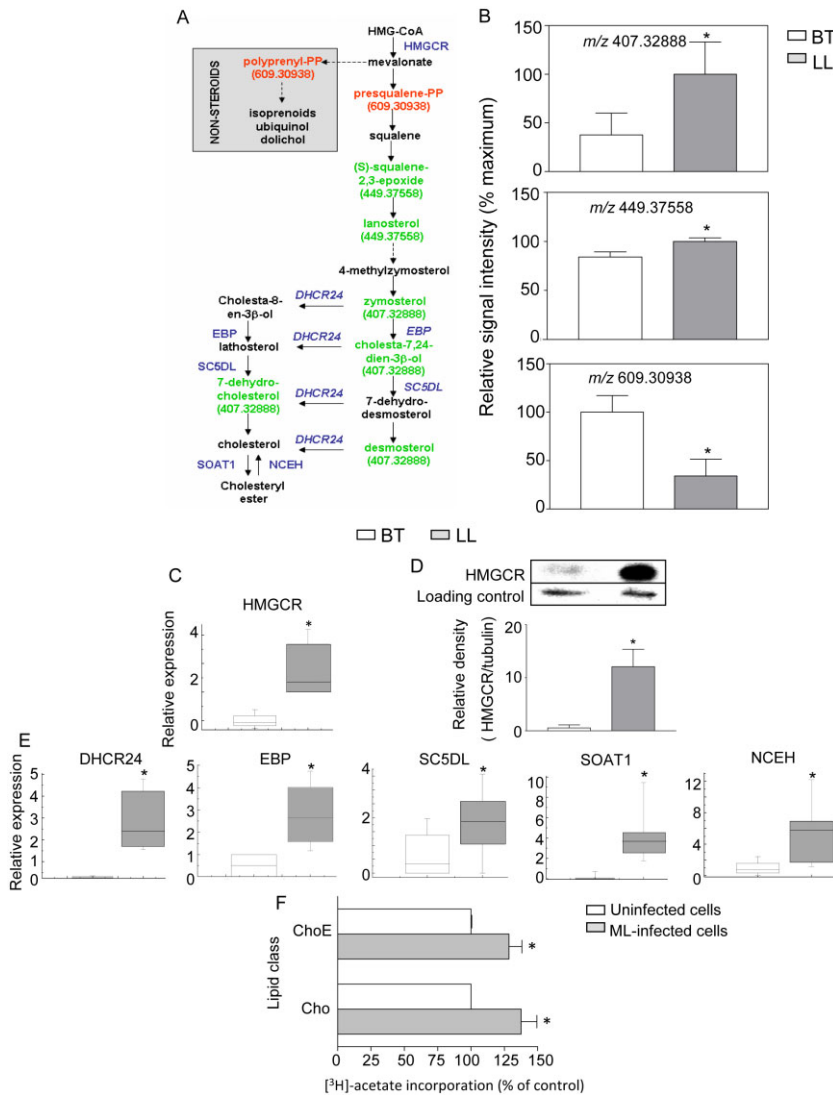
Fig. 2. Modulation of host steroid metabolism during ML infection.
A. Steroid biosynthetic pathway in humans. Metabolites present at different levels in BT and LL samples are coloured red (higher in BT samples) and green (higher in LL samples), and their *m/z* values are indicated within parentheses.
B. Signal intensity values of metabolites indicated in (A). White columns indicate average signal intensities from BT samples whereas grey columns indicate average intensity values from LL samples. Bars indicate the standard errors of means.
C and D. HMGCR expression in leprosy skin biopsies. (C) Total RNA was extracted from BT and LL biopsies and the expression of HMGCR was quantified by qRT-PCR, being normalized to GADPH levels. Values are the average of four independent experiments. (D) Cell lysates (30 µg of protein) were subjected to SDS-PAGE and analysed by Western blot with anti-HMGCR and anti-β-tubulin antibodies. The figure shows a representative Western blot. The graph shows the normalized values (tubulin) from three independent experiments.
E. Total RNA was isolated from BT and LL skin biopsies and subjected to qRT-PCR analysis to measure the enzymes from the *de novo* Cho pathway as shown in (A).
F. Acetate incorporation was assayed in uninfected and ML-infected macrophages after 48 h. Incorporation of [^{3}H] acetate into the cholesterol (Cho) and cholesteryl ester (ChoE) was measured in counts per minute of [^{3}H] acetate incorporated into 10^6 macrophages and expressed as percentages relative to the control (uninfected cells) ± SEM from three separate experiments.
Statistically significant differences were at $P \leq 0.05$ when the BT group was compared to the LL group and uninfected cultures to ML-infected cells. *Statistically significant differences ($P \leq 0.05$) comparing LL with BT. Statistically significant differences ($P \leq 0.05$) comparing ML-stimulated versus control cells.

metabolomic analysis of human skin biopsies from four LL and four BT patients. To do so, metabolites were extracted from the biopsies and the composition of each sample was analysed through DI-FT-ICR MS. These procedures made it possible to detect almost 2000 metabolites, whose relative abundance in LL versus BT lesions was compared.

Among the metabolites with different levels between BT and LL biopsies, three were identified as corresponding to metabolites of the human steroid biosynthetic pathway (Fig. 2A). *m/z* 609.30938 was present at higher levels in the BT samples (Fig. 2B). This *m/z* may correspond to two distinct metabolites: presqualene-PP (steroid pathway) and polyprenyl-PP (terpenoid-quinone biosynthesis pathway). Conversely, *m/z* 407.32888, which may correspond to four different metabolites in the steroid pathway

(zymosterol, cholesta-7,24-dien-3β-ol, desmosterol, and 7-dehydro-cholesterol), and *m/z* 449.37558, which may correspond to two possible metabolites [(S)-squalene-2,3-epoxide, and lanosterol], were present at higher levels in LL samples (Fig. 2B). The possible accumulation of presqualene-PP in the steroid pathway and polyprenyl-PP in the terpenoid-quinone biosynthesis pathway suggests that the precursor of steroid pathways can be re-directed to a non-steroidal pathway at the BT pole (Fig. 2A). On the other hand, steroid end-products of this metabolic pathway that culminate in Cho biosynthesis seem to accumulate in LL, suggesting a shift to steroid metabolism during ML infections, in accordance with the clinical form of the disease. The metabolomic data were validated by measuring the expression of a selected group of enzymes in the Cho pathway in LL and BT lesions.

Hydroxy-3-methyl-glutaryl-CoA reductase (HMGCR), a critical enzyme of the Cho biosynthetic pathway, was found in higher levels in LL samples, both at the mRNA (~ 1.6-fold, $P = 0.0076$) and at protein levels (~ 21-fold, $P = 0.02$), as shown by qRT-PCR and Western blot respectively (Fig. 2C and D). The expression levels of other enzymes in the Cho biosynthetic pathway were investigated by qRT-PCR: 24-dehydrocholesterol reductase (DHCR24), 3 hydroxysteroid-delta 8-delta 7-isomerase beta (EBP), and sterol-C5-desaturase-like (SC5DL). As shown in Fig. 2E, these genes were upregulated in LL in comparison to BT lesions. Moreover, O-acyltransferase 1 (SOAT) and neutral cholesterol ester hydrolase (NCEH), enzymes involved in ChoE formation and hydrolysis, respectively, were also found in increased levels in LL lesions (Fig. 2E). Therefore, as inferred by the metabolomic analysis, qRT-PCR and Western blot data corroborated the modulation of the Cho pathway in LL versus BT biopsies.

To confirm that ML-infected macrophages display higher cholesterogenic activity, we analysed the lipid extracts obtained after pulsing the cells with [³H] acetate. Radiolabelled profiles showed that infected macrophages are capable of synthesizing higher levels of Cho (~ 1.3-fold, $P = 0.04$) and ChoE (~ 1.4-fold, $P = 0.03$) than uninfected cells (Fig. 2F). In conjunction with the upregulation of the enzymes in the Cho biosynthetic pathway and the increased levels of Cho precursors found in LL skin biopsies, this result indicates that the accumulation of Cho in the foamy macrophages present at this disease pole is derived, at least in part, from the *de novo* synthesis of Cho induced by ML infection.

ML infection increases the uptake of LDL-cholesterol by macrophages

Besides the *de novo* Cho synthesis, the extracellular uptake of plasma lipoprotein-derived Cho may be an alternative lipid source of the foamy aspect of LL lesions. We then investigated whether *in vitro* infected macrophages show an increased capacity to uptake native LDL (LDL-Cho). Uninfected or ML-infected macrophage cultures were first incubated with or without LDL-Cho, and Cho cellular levels were determined either by staining the cells with filipin followed by flow cytometry analysis (Fig. 3A), or by a fluorimetric assay kit (Fig. 3B). The addition of (0.1 mg ml⁻¹) LDL-Cho to uninfected macrophages did not cause any changes in Cho levels, in contrast to the increased levels observed in infected cultures (Fig. 3A and B). This result suggests that ML is able to dysregulate host cell Cho homeostasis by increasing the uptake of native LDL-Cho.

This pathway was further investigated by monitoring the cellular internalization of fluorescent LDL-[BODIPY-Cho]. Cells kept in serum-free medium and infected for 48 h were pulsed with LDL-[BODIPY-Cho] and lipid uptake was analysed after 2 h of treatment by flow cytometry. LDL uptake was higher in ML-infected cells than in cells treated with dead bacteria and in uninfected cultures (MFI of 33.2 ± 2.3 in live ML-infected cells, 16.3 ± 1.9 in dead ML-treated cells and 12.8 ± 0.33 in uninfected cells, $P = 0.001$) (Fig. 3C). Similar results were obtained when cells were incubated with LDL-[³H]-Cho in replace to LDL-[BODIPY-Cho] (cpm mg⁻¹ cell protein of 2743 ± 652.4 in live ML-infected cells, 1956 ± 555.2 in dead ML-treated cells and 1259 ± 136.3 in uninfected cells, $P = 0.05$, Fig. 3D). Furthermore, as shown in Fig. 3E, a dose–response relationship between bacterial infection and LDL-[BODIPY-Cho] incorporation was observed [MFI of 12.5 ± 0.3 in control cells to 22.6 ± 2.4 at multiplicity of infection (moi) 2.5, $P = 0.003$, and 33.0 ± 2.7 at moi 5, $P = 0.003$]. Interestingly, the increased uptake of native LDL-Cho by ML-treated cells seems to be more efficiently induced by viable organisms since, although apparently higher levels were also observed with dead bacteria, the differences with the control cells did not reach statistical significance (Fig. 3C and D). This is not observed when total Cho levels were measured, both dead and viable bacteria inducing higher comparative Cho accumulation in the host cell (μg mg⁻¹ cell protein of 1.206 ± 0.08 in live ML-infected cells, 1.152 ± 0.1 in dead ML-treated cells and 0.6628 ± 0.04 in uninfected cells, $P < 0.0001$ and $P = 0.0003$, respectively, Fig. S1). This is in agreement with our previous results indicating that ML is able to induce LD biogenesis in macrophages independent of bacterial viability (Mattos *et al.*, 2010) and reinforce the idea that multiple mechanisms collaborate with Cho accumulation in macrophages treated with ML.

To verify whether the effect of ML on Cho uptake described herein was restricted to bacteria-bearing cells, untreated cells or those exposed to PKH26-labelled ML were cultured for 48 h, pulsed with LDL-[BODIPY-Cho] for 2 h, and Cho uptake was measured by flow cytometry. The observed cellular fluorescent intensity of LDL-[BODIPY-Cho] was significantly higher in bacteria-bearing cells compared to cells with no bacteria (MFI of 8.56 ± 1.0 in control cells to 16.6 ± 0.8 in ML-negative cells, $P = 0.004$ and 246.4 ± 72.9 in ML-positive cells, $P = 0.03$, Fig. 3F). These data were confirmed by immunofluorescence images that clearly showed intense fluorescence of LDL-[BODIPY-Cho] in ML-bearing cells. However, cells that had not internalized ML also internalized the fluorophore, resulting in weak labelling (Fig. 3G). In the end, this profile of intense lipid accumulation found predominantly in ML-bearing cells was confirmed in isolated Virchow's cells. As shown in Fig. 3H, accumulation of LDL-[BODIPY-Cho] was notably observed in highly infected macrophages but not in neighbouring cells without internalized ML. Taken together, these results
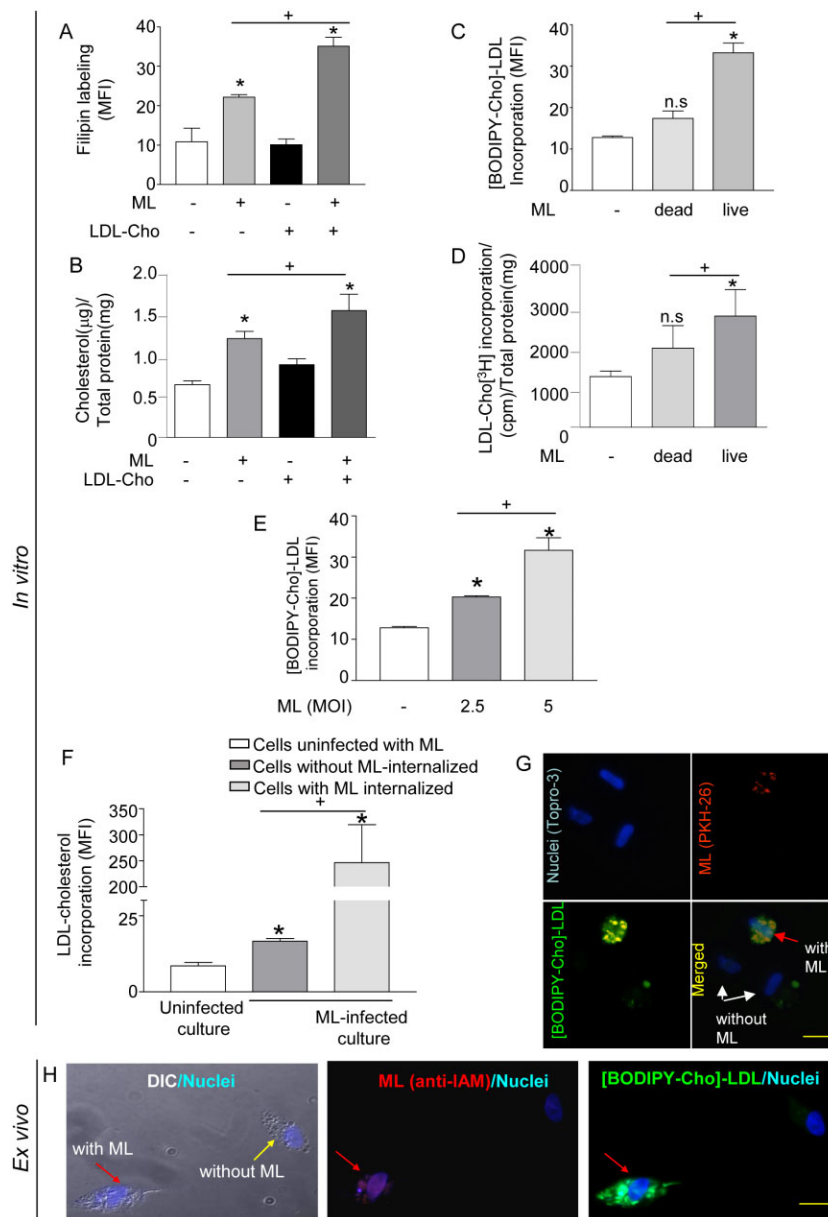
Fig. 3. Cellular incorporation of LDL-cholesterol in ML-infected macrophages. Forty-eight hours after infection in medium containing 2% FCS, infected macrophages were pulse-labelled at 33°C with LDL-Cho for 2 h in medium serum free.

A. The effect of native LDL-Cho and ML infection on intracellular Cho levels measured by filipin staining and flow cytometry.

B. In parallel, the quantitative analysis of total Cho was determined by Amplex Red Cholesterol kit under the same conditions.

C. Cells were treated with dead or live bacteria in the same condition described above and the LDL-[BODIPY-Cho] incorporation was determined by flow cytometry.

D. To validate the fluorescence assay the LDL-[^{3}H]-Cho incorporation was assayed under same condition of fluorescence assay.

C–E. The internalization of LDL-[BODIPY-Cho] as a process dependent on bacterial viability (C and D) and multiplicity of infection (moi) (E) as determined by flow cytometry.

F. Bacterial association and LDL-[BODIPY-Cho] were measured simultaneously by flow cytometry. A separate analysis was performed in cells with no bacteria (cells without internalized ML) and cells bearing bacteria (cells with internalized ML). MFI values of LDL-[BODIPY-Cho] are expressed in bar graphs.

Results from five representative experiments are shown. *Statistically significant differences ($P \leq 0.05$) when comparing ML-infected cells with control cells. +Statistically significant differences ($P \leq 0.05$) when comparing different ML-treated cell groups; n.s: non-significant.

G and H. Fluorescence images of macrophage cultures showing LDL-[BODIPY-Cho] in cells associated or not with ML. (G) Macrophages isolated from PBMC and (H) Virchow cells isolated from LL skin biopsies. Original bar, 10 μm.

indicate that ML infection increases the uptake of exogenous LDL-Cho in macrophages, thereby contributing to their foamy phenotype.

ML infection induces the in vivo *and* in vitro *expression of LDL receptors*

The cellular uptake of plasma LDL occurs by way of a receptor-mediated endocytosis process via the receptor for native-LDL (LDL-R) in addition to the scavenger receptors for modified LDL: cluster of differentiation 36 (CD36), scavenger receptor class A (SR-A1), scavenger receptor class B type I (SR-B1), and LDLR-related protein 1 (LRP-1). The expression of classical lipoprotein receptors was

then evaluated by qRT-PCR in LL and BT lesions. As shown in Fig. 4A, SR-A1, SR-B1, LRP-1 and LDL-R are upregulated in LL in contrast to BT lesions. The LDL-R is the primary pathway for removal of Cho from the circulation and its induction in LL lesions was confirmed at the protein level by Western blotting (Fig. 4C). The higher expression of the two best-studied receptor for oxidized LDL, SR-A1 and CD36 in LL skin biopsies were also confirmed at the protein level. The expression and distribution of SRA in leprosy skin lesions (BT, $n = 4$; LL, $n = 4$), was determined by immunohistochemistry. In BT skin lesions, SR-A1 was observed only in inflammatory infiltrates and sometimes in the papillary dermis nearly to epidermis. In contrast, LL skin lesions presented higher
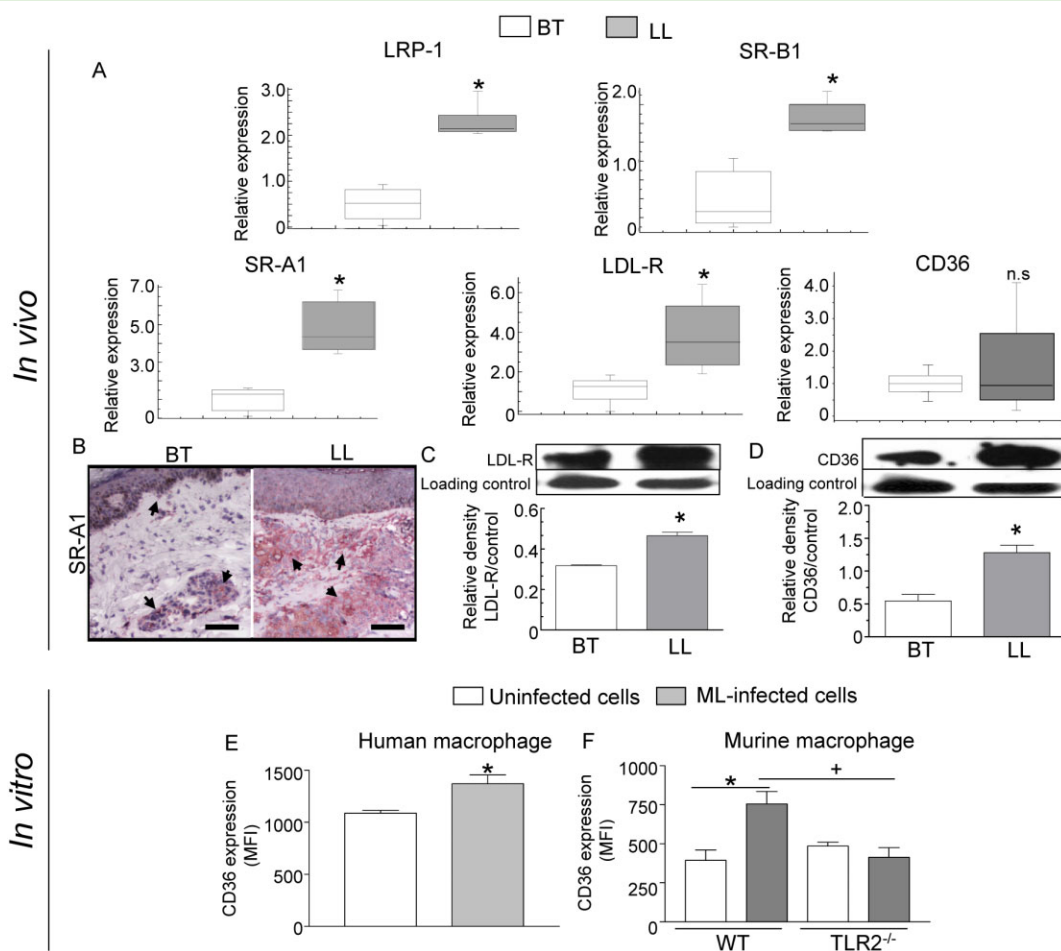
Fig. 4. LDL receptors are upregulated by ML infection of human macrophages.
A. Total RNA was isolated from LL and BT skin biopsies and subjected to qRT-PCR analysis to measure LDLR, LRP-1, SR-A1, SR-B1, CD-36 and GADPH mRNA expression. Values are the average of four independent experiments.
B. Leprosy lesions were labelled with the monoclonal antibody SR-A1. Shown are representative sections from LL and BT lesions. In BT skin lesions the distribution of few SR-A1+ cells was concentrated in inflammatory infiltrates and nearly to epidermis (arrows). LL skin lesions presented a higher positive SR-A1 cells within the dermis, mainly in inflammatory infiltrates (arrows). Photomicrographs are representative of four experiments performed. Scale bar: 50 μm.
C and D. Cell lysates (20 μg of protein) were subjected to SDS-PAGE and analysed by Western blot with anti-LDL-R (C), anti-CD36 (D) and as loading control, anti-GADPH antibodies (C–D). The figure shows a representative Western blot. The graph shows the normalized values (GADPH) from three independent experiments.
E and F. (E) CD36 expression in human macrophages and (F) WT and TLR2$^{-/-}$ murine macrophages was performed using flow cytometry.
*$P \leq 0.05$, ML-stimulated versus control cells and LL versus BT groups. +$P \leq 0.05$ between the different ML-treated cell groups.

numbers of SR-A1+ cells distributed in inflammatory infiltrates bound in the entire dermis (Fig. 4B). A Western blot analysis of CD36 showed higher levels of this receptor in LL lesions than in BT lesions (Fig. 4D). Corroborating with *in vivo* results, higher protein levels of this scavenger receptor were detected in macrophages infected *in vitro* with ML (Fig. 4E and F). As shown in Fig. 4E, human macrophages infected with ML for 48 h showed a significantly higher expression of CD36 (MFI of 1089 ± 26.03 in uninfected cells and 1371 ± 84.51 in ML-infected cells). These data suggest that the increased uptake of native and modified LDL may contribute to the accumulation of

Cho in the ML-infected macrophage cells due to the increased gene expression in several classes of LDL receptors.

Since we have previously shown that TLR2 is essential for the induction of the foamy phenotype in ML-infected macrophages (Mattos *et al.*, 2010), we next assessed whether ML-induced upregulation of CD36 relies on TLR2 signalling by comparing CD36 expression in *in vitro* infected macrophages derived from WT versus TLR2$^{-/-}$ mice. As shown in Fig. 4F, in contrast to WT macrophages (MIF of 394.0 ± 66.57 in uninfected cells and 754.7 ± 79.6 in ML-infected cells $P = 0.0255$), no increase in CD36
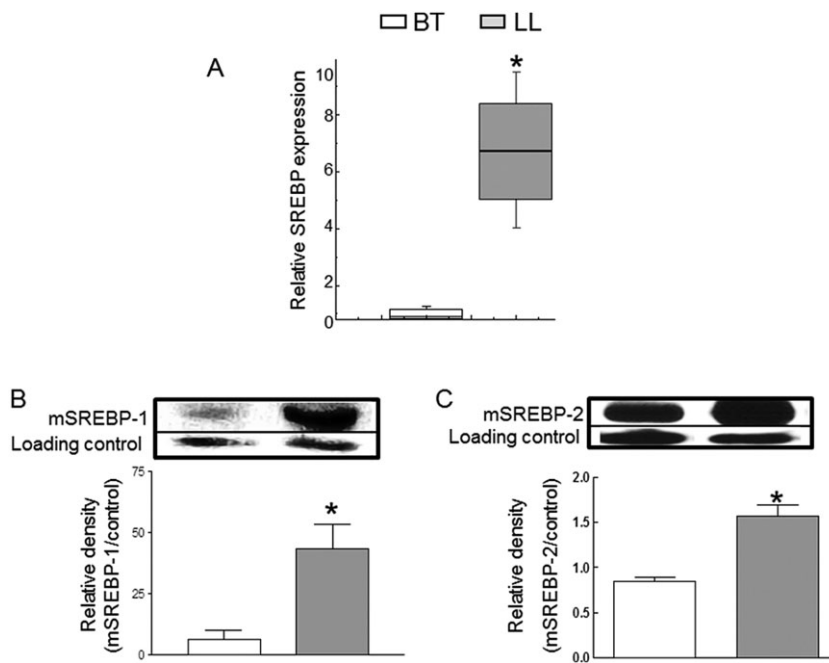
Fig. 5. ML *in vivo* infection induces SREBP expression and activation.
A. The expression of SREBPs was compared in skin biopsies of LL versus BT of leprosy patients by qRT-PCR.
B and C. Total RNA was extracted from BT and LL biopsies and the expression of SREBP was quantified by qRT-PCR, being normalized to loading controls α-tubulin (B) and GADPH (C) levels. The levels of the activated/mature forms (mSREBP) of both SREBP-1 (B) and SREBP-2 (C) were analysed by Western blot.
The figure shows a representative Western blot. The graph shows the normalized values (loading control) from three independent experiments. *$P \leq 0.05$.

expression was observed in TLR2$^{-/-}$ null ML-infected cells (MIF of 484.3 ± 25.90 in uninfected cells and 413 ± 62.4 in ML-infected cells $P = 0.3527$), showing that ML-induced CD36 is TLR2-dependent (MIF of 754.7 ± 79.6 in WT cells and 413 ± 62.4 in TLR2$^{-/-}$ cells, $P = 0.0279$). These results indicate that ML-mediated upregulation of CD36 relies on TLR2 signalling, and may partially explain the dependence of ML-induced foamy macrophages on this receptor (Mattos *et al.*, 2010).

Members of the sterol regulatory element-binding protein (SREBP) transcriptional factors regulate the biosynthesis and uptake of cholesterol (Goldstein *et al.*, 2006; Jeon and Osborne, 2012). Given the accumulation of Cho and ChoE in ML-infected tissues, we hypothesized that SREBPs could be involved in the regulation of host lipid metabolism during the course of leprosy. By using qRT-PCR, we observed that SREBP mRNA was highly upregulated in LL as opposed to BT biopsies (Fig. 5A). In addition, Western blot analysis of skin biopsies showed that the active/mature form (mSREBP) of both SREBP-1 (Fig. 5B) and SREBP-2 (Fig. 5C) are present at higher levels in LL than in BT lesions. In conclusion, the data generated in this section of the study suggest that ML induces a foamy phenotype in infected cells through activation of SREBPs transcriptional factors.

The itinerary of cholesterol: from extracellular sources and lipid droplets to ML-containing phagosomes

As a follow-up to the results described above, we decided to look into the accessibility of the accumulated Cho to intracellular ML. Confocal microscopy was used to monitor the association of ML with LDs, organelles that are well known for storing excess intracellular Cho. To this end, LL skin biopsies were double stained for bacteria, with anti-LAM, and for LDs, with anti-ADRP, showing a colocalization of ML to LDs (Fig. 6A and B, inset, yellow arrow). Isotype controls are shown in Fig. S2A. To investigate this association in more detail, Virchow's cells were isolated from LL skin biopsies. The lipid-laden, a hallmark of this cell type, was highlighted by Oil red O staining (Fig. 6C). To characterize the chemical nature of the lipids detected in close association with ML, Virchow's cells were labelled with filipin, and ML, using anti-LAM (Fig. 6D and E), which revealed accumulated Cho surrounding the bacterial phagosome (Fig. 6D, inset, yellow arrow). As Cho is accumulated in LD organelles, we then investigated the LD-ML association using BODIPY (Fig. 6F) or anti-ADRP (Fig. 6G) labelling to visualize the LD organelles, and anti-LAM to identify the bacteria. Isotype controls are shown in Fig. S2B. As shown in Fig. 6F and G, these cells adopted the same pattern observed in LL skin biopsies in view of the close association between LDs and ML observed in Virchow's cells. Interestingly, the green fluorescent pattern surrounding ML adopted the bacterial shape (Fig. 6G, inset, yellow arrow) as opposed to the classical spherical shape assumed by LDs when free in the cytoplasm, indicating an intimate association with ML-containing phagosomes, as was previously detected in ML-infected Schwann cells (Mattos *et al.*, 2011a).

We also evaluated the traffic of exogenous LDL-[BODIPY-Cho] in infected macrophages isolated from LL biopsies (Virchow's cells) by confocal analysis. Cells were pulsed with LDL-[BODIPY-Cho] for 2 h, as previously
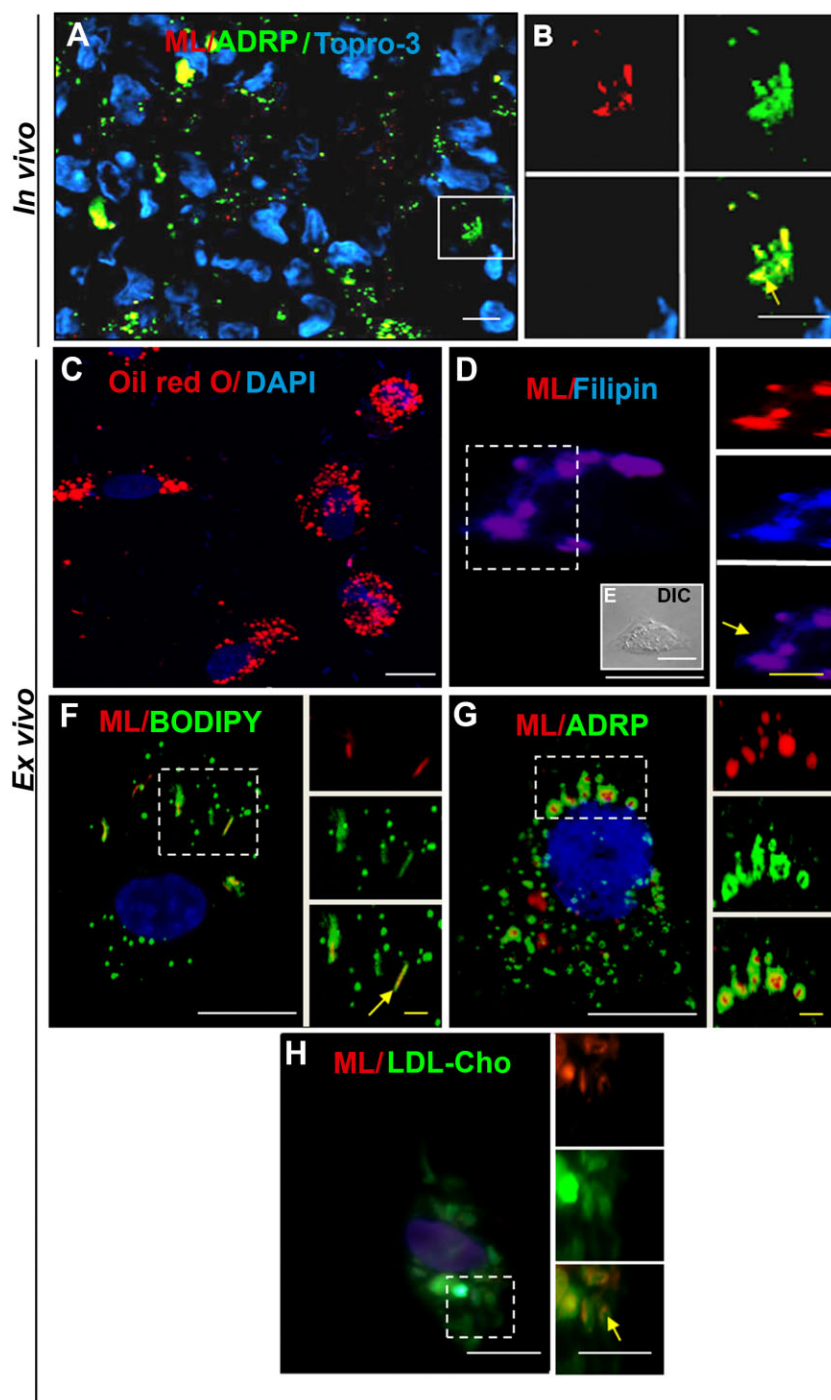
Fig. 6. Intracellular cholesterol sources colocalize with ML in foamy macrophages of LL patients.
A. Sections of skin biopsies of LL patients (*n* = 4) were analysed showing colocalization between LD organelles (green) and ML (red).
B. High magnification of the boxed areas visualized in (A) showing bacteria completely enveloped by LDs (yellow arrow).
C–H. Virchow's cells isolated from LL biopsies were stained with different fluorophores and anti-ADRP to visualize Cho sources within these ML-infected foamy macrophages. (C) Oil red O reveals the foamy phenotype of the isolated Virchow's cell. (D) Fluorescence and (E) Differential interference contrast (DIC) of a Virchow's cell showing ML residing in Cho-rich regions (yellow arrow). (F) LD–ML association within macrophages isolated from LL biopsies was visualized using BODIPY label. (G) Immunofluorescence confocal images for ADRP (green) and anti-LAM (red) show the LD–ML association (yellow arrow) (H) LDL-[BODIPY-Cho] internalization in Virchow's cells and intimate association with ML (yellow arrow). Nuclei were stained with TO-PRO-3. No fluorescence was observed with the isotype control IgG (Supplementary Fig. S2). Bars: white = 10 mm; yellow = 5 mm. Filipin was used as a Cho label (blue). BODIPY and ADRP were used as LD marker (green); LDL-Cho: LDL fluorescent as LDL-[BODIPY-Cho] (green), LAM (lipoarabinomannan) was used as an ML marker (red).

mentioned. Images showed the predominant labelling of LDL-[BODIPY-Cho] in highly infected macrophages. These images also showed isolated, well-circumscribed bacilli enveloped by LDL labelling (Fig. 6H), suggesting that internalized bacteria trigger a recruitment process of this lipid source towards ML-containing phagosomes similar to the one observed in relation to LD organelles (Fig. 6G). Taken together, these results show a close association between Cho sources and ML within infected macrophages, indicating that the pathogen most likely has abundant access to this compound in its intracellular niche.

As a final step, LL skin biopsies were processed for transmission electron microscopy (TEM). ML-infected macrophages cells exhibited large phagosomes containing many bacteria (Fig. 7A and B). Typical round LDs
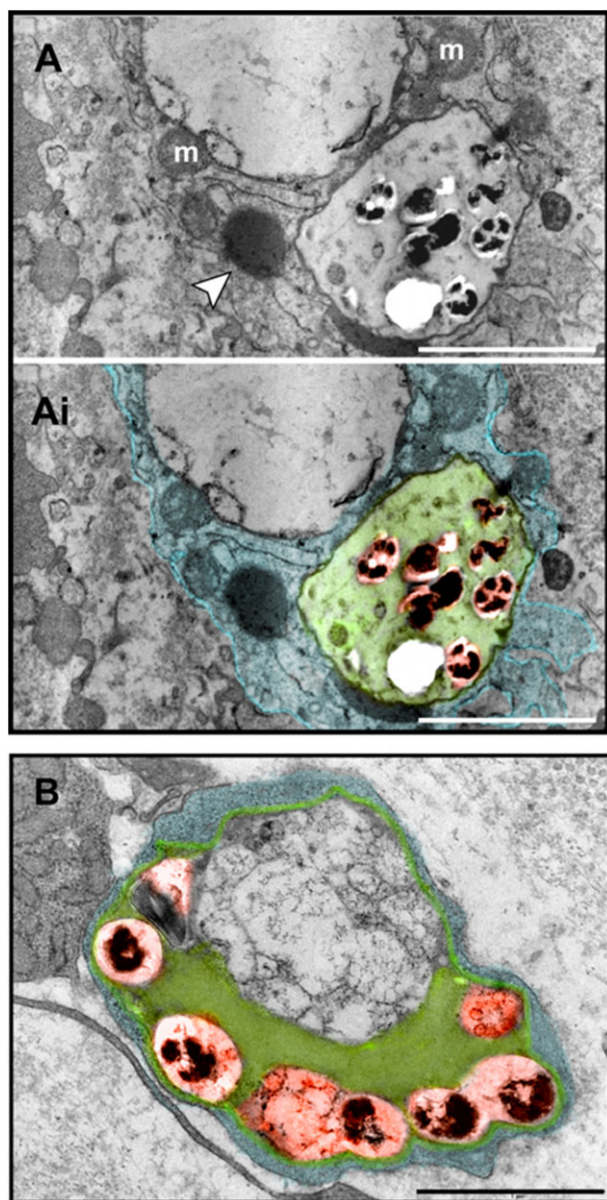
Fig. 7. Transmission electron microscopy of a LL skin biopsy showing *Mycobacterium leprae*-infected macrophages.
A and B. Large phagosomes in the macrophage cytoplasm show several bacilli (highlighted in red in Ai and B) enmeshed in a lipid content (highlighted in green in Ai and B). Arrowhead in (A) indicates a typical lipid droplet in association with a phagosome. m, mitochondrium. Bars = 2 μm (A); 1 μm (B).

(Fig. 7A, arrowhead) were found in the macrophage cytoplasm in close association with phagosomes. Moreover, an amorphous material indicative of accumulated lipid was also observed within these vacuoles as previously demonstrated by TEM within ML-containing phagosomes in Schwann cells (Mattos *et al.*, 2011a). Bacteria were clearly enmeshed in the lipid content (Fig. 7A, Ai and B) confirming our present data provided by confocal microscopy analysis of isolated Virchow's cells (Fig. 6D–H).

Intracellular survival of ML depends on cholesterol accumulation in infected macrophages

Accumulating evidence suggests that host lipid modulation may favour intracellular mycobacterial survival and/or replication (D'Avila *et al.*, 2008; Almeida *et al.*, 2009; Mattos *et al.*, 2010; 2011a,b; van der Meer-Janssen *et al.*, 2010). Therefore, a question remained as to whether the higher Cho levels observed in ML-infected macrophages favour intracellular bacterial survival. Infected cells were then incubated in the presence (medium plus FCS) or absence (AIM V medium) of FCS, a source of exogenous Cho, and treated or not with lovastatin, an inhibitor of *de novo* Cho biosynthesis. The strategies used to alter cellular Cho metabolism are summarized in Fig. S3. After incubation for 72 h, mycobacterial viability was assessed by flow cytometry via the LIVE/DEAD Bactlight Bacterial Viability Kit. The levels of host cell viability were similar in all conditions (data not shown). ML-infected macrophages cultivated in RPMI medium supplemented with serum (FCS) and treated with lovastatin showed lower Oil red O staining (Fig. 8A) and reduced Cho levels, as shown by HPTLC analysis (Fig. 8B) and enzymatic method for Cho quantification (Fig. 8C). In these conditions, a reduction of more than 90% in ML viability compared with untreated cultures was observed despite the presence of an exogenous Cho source provided by the serum (FCS), seen in Fig. 8D. Bacterial survival was also assayed in the defined serum-free AIM V medium. The absence of an LDL source in AIM V medium alone caused a reduction of approximately 50% in ML viability when compared to cells cultivated in RPMI plus FCS. This result suggests that exogenous LDL is required at least in part for intracellular mycobacterial survival. However, a drastic effect was observed in ML viability when macrophages were cultured in AIM V treated with lovastatin (~ 90% reduction in ML viability). Of note, lovastatin was able to inhibit ML viability even in the presence of exogenous lipid sources, suggesting that the drug may also interfere with LDL uptake. Indeed, ML-infected macrophages in AIM V medium showed a twofold decrease in the binding/incorporation capacity of LDL-[BODIPY-Cho], twofold less than when treated with lovastatin (MIF of 11.9 ± 9.0 in untreated cultures to 6.0 ± 1.0 in cultures treated with lovastatin, $P = 0.015$, Fig. S4). Thus, these data suggest that lovastatin may decrease cellular Cho concentration in ML-infected macrophages by acting in two different moments of Cho metabolism: inhibiting HMGCR and decreasing exogenous Cho uptake.

Similar assays were also conducted with BCG, used as a model for *M. tuberculosis* infection, since this mycobacterial species was previously reported to utilize host lipids for intracellular persistence (D'Avila *et al.*, 2006; Almeida *et al.*, 2009; Brzostek *et al.*, 2009). Human
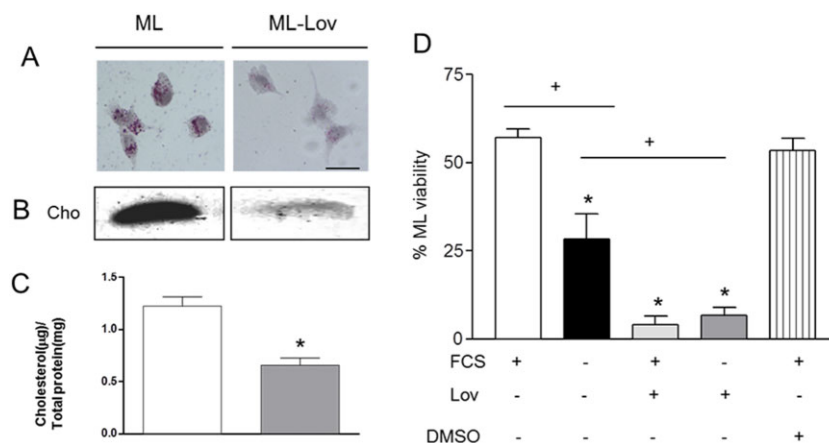
Fig. 8. Intracellular mycobacterial viability is dependent on exogenous and endogenous host cholesterol.
A. Phenotype of monocytes isolated from PBMC and infected with ML, treated and not with statin (72 h), was visualized by Oil red O. Bars: 20 mm.
B and C. (B) Cho levels extracted from ML-infected monocytes treated or not with statin was determined by HPTLC and by (C) the quantitative analysis determined by Amplex Red Cholesterol kit under the same conditions.
D. Monocytes were infected with ML, treated or not with statin, and depleted of LDL from serum (serum-free AIM V medium) or not (RPMI supplemented with FCS) to determine the role of Cho in mycobacterial survival. Percentage of live and dead bacteria was evaluated using the LIVE/DEAD BacLight Bacterial Viability Kit in combination with flow cytometry. Statistically significant ($P \leq 0.05$) differences between control and drug-treated groups are indicated by asterisks and + between different drug-treated groups.

macrophages were infected with BCG and then submitted to different culture conditions, namely RPMI medium supplemented with: LDL-depleted serum (dLDL; removal of the exogenous Cho source), lovastatin (inhibition of the *de novo* synthesis of Cho), or both simultaneously (Fig. S3). As shown in Fig. S5, incubating the cells in dLDL significantly reduced the percentage of live intracellular BCG as compared to the control cultures (cells treated with FCS) (MFI of 84.5 ± 2.7 in FCS-treated cells and 58.9 ± 3.0 in dLDL-treated cells). BCG showed reduced viability when cells were treated with lovastatin, and this reduction was similar to the one observed in cells incubated with dLDL (MFI of 63.4 ± 0.7). This reduction, however, was not observed in cells incubated with vehicle only (DMSO), (MFI of 76.4 ± 6.2). Depletion of host exogenous and endogenous Cho sources simultaneously (medium with dLDL plus lovastatin) led to an even higher reduction in BCG viability (MFI of 45.2 ± 2.4). The additional decrease in bacterial viability found in this condition was prevented by feeding the cells with exogenous steroid lipid molecules such as free Cho or ergosterol, as described by Av-Gay and Sobouti (2000). These data suggest that both sources of Cho (exogenous and endogenously generated Cho via biosynthesis) play a role in favouring BCG survival inside macrophages. The levels of host cell viability were similar in all conditions.

Discussion

A vast body of evidence indicates that lipid-laden, infected cells perform a key pathophysiological role in tuberculosis and leprosy (Peyron *et al.*, 2008; Bozza *et al.*, 2009; Elamin *et al.*, 2012; de Mattos *et al.*, 2012; Saka and Valdivia, 2012; Singh *et al.*, 2012). In view of the importance of this foamy phenotype in mycobacterial disease, an investigation was undertaken into the cellular mechanisms triggered by ML to display this shift in lipid metabolism in infected macrophages. Based on the analysis of leprosy skin lesions, which was complemented by *ex vivo* experiments with isolated infected macrophage cells from LL biopsies (Virchow's cells) and *in vitro* experiments with human and murine macrophages, we concluded that ML is able to disrupt the cellular Cho homeostasis leading to Cho accumulation in infected cells. One way through which ML induces Cho accumulation is by stimulating the *de novo* Cho synthesis pathway. This was demonstrated by the higher expression levels of critical enzymes of *de novo* Cho biosynthesis in LL lesions complemented by functional assays *in vitro* that confirmed an increased capacity on the part of infected macrophages to synthesize Cho from acetate.

Besides increasing endogenous Cho synthesis, it was seen that ML relies on a second mechanism to induce intracellular Cho accumulation. This mechanism involves increasing the uptake of exogenous sources of Cho via upregulation of LDL receptors. *In vitro* and *ex vivo* assays clearly showed that ML-infected macrophages avidly capture native LDL, which is not the case for uninfected cells. Moreover, we showed an increase in levels of CD36, the major oxLDL receptor of macrophages, in *in vitro* ML-infected cells. This is in concert with recent

reports suggesting the role of oxidized phospholipids and the CD36 scavenger receptor on the foamy aspect of ML-infected macrophages in LL lesions (Cruz *et al.*, 2008; Montoya *et al.*, 2009). In addition, we demonstrated that the expression of LDLR, LRP-1, SR-A1, SR-B1 and CD36 were upregulated in LL but not in BT lesions, insinuating that both native and modified lipoproteins may also contribute to the foamy phenotype observed in leprosy.

One essential component in the cascade signalling trigged by ML to dysregulate the cellular Cho homeostasis seems to be the TLR2 receptor since TLR2-null macrophages were unable to express higher levels of CD36, as shown herein, or LDs in response to ML, as previously described (Mattos *et al.*, 2010). Of note, a cooperation between TLR2 and CD36 in BCG-induced LD formation has been recently described (Almeida *et al.*, 2014).

The downstream transcription factors in ML-induced Cho accumulation and foam-cell formation in human macrophages was likewise investigated. Our demonstration that SREBP mRNA is upregulated as well as the increased levels of active/mature form of both SREBP-1 and SREBP-2 in LL as opposed to BT biopsies strongly suggest the involvement of SREBPs ML-induced Cho accumulation and LD formation. Indeed, SREBPs activation upregulates a set of genes involved in Cho *de novo* synthesis and uptake, such as HMGCR and LDLR (Espenshade, 2006; Goldstein *et al.*, 2006; Jeon and Osborne, 2012). However, the signalling pathways involved in this dysregulation need further investigation.

The intimate physical association between LDs, organelles enriched in Cho, and intracellular ML corroborates previous findings (Tanigawa *et al.*, 2008; Mattos *et al.*, 2010) and correlates with our recent observations in ML-infected SCs (Mattos *et al.*, 2011a), pointing to these organelles as potential Cho sources for ML. Moreover, upon LDL-[BODIPY-Cho] uptake, the region of the bacterial phagosome in Virchow's cells was markedly labelled, indicating that Cho internalized as LDL-Cho is predominantly re-directed to the bacterial compartment in ML-infected macrophages. These data suggest that intracellular ML guarantees an abundant supply of Cho by at least two alternative mechanisms: (i) via recruiting early endosomes containing recently endocytosed exogenous LDL and (ii) through sequestering accumulated lipids from LD organelles. Furthermore, the upregulation of SOAT and NCEH enzymes by ML suggests an active interchange and high mobilization of Cho/ChoE stocks in infected cells. Based on the data presented herein, we propose that ML localization in high-Cho regions constitutes an efficient strategy of intracellular ML to acquire host macrophage lipids and promote bacterial survival. How ML translocates Cho to its own cytoplasm and

whether this lipid can be utilized as carbon and energy sources remains to be established.

A very exciting finding has to do with the capacity of lovastatin to favour macrophage killing of intracellular ML, corroborating the results indicating that ML is able to disrupt Cho cellular homeostasis. The effect of statins on intracellular ML was recently confirmed by using an alternative bacterial viability method based on quantification of 16S ribosomal RNA by qRT-PCR. Moreover, statins were shown to control *in vivo* ML infection in the Shepard model (L. Lobato, unpubl. results). This is in concert with several reports suggesting that host lipid acquisition during infection is a key aspect in mycobacterial pathogenesis. The capacity of *M. tuberculosis* to maintain a chronic infection has been shown to be critically linked to its ability to acquire Cho from the host (Pandey and Sassetti, 2008). Mycobacterial persistence requires the utilization of host Cho. We and others have previously shown that the inhibition of LD formation in ML- and BCG-infected cells reduces bacterial viability (D'Avila *et al.*, 2006; Almeida *et al.*, 2009; Mattos *et al.*, 2011b). Moreover, a recent report has suggested that clofazimine, one of the drugs that compose the WHO-MDT regimen for leprosy treatment, exerts its microbicidal activity via the decreasing LD accumulation in infected cells (Degang *et al.*, 2012). Interestingly, besides its classical mechanistic action of inhibiting the HMGCR, lovastatin was able to decrease LDL-Cho uptake in ML-infected macrophages, corroborating with the literature data (Aviram *et al.*, 1991). Of note, lovastatin was shown to more drastically affect ML viability than BCG viability. However, in a recent study using two different statins, atorvastatin and simvastatin, and monitoring bacterial viability by cfu counting inside THP cells, BCG was killed as efficiently as ML by these drugs (L. Lobato *et al.*, unpubl. results). These controvert results indicate the need of a more careful analysis of the potential higher susceptibility of ML to statins in comparison to other mycobacterial species. Finally, our data on the killing effect of statins on ML and BCG is reinforced by a recent study published while our manuscript was under revision that shows a similar effect of these drugs on Mtb (Parihar *et al.*, 2014).

Although widely accepted, the current multidrug therapy in use for leprosy treatment (WHO-MDT) demands a number of improvements for several reasons. In addition to its many adverse effects that must be addressed, treatment is exceedingly long, reports of relapses are frequent, and drug-resistant ML strains have emerged (Prasad and Kaviarasan, 2010). Thus, the general consensus is that there is an urgent need for new drugs that could lead to improvements in the outcomes of leprosy therapy. Based on the data presented, statins could be proposed as an additional viable drug for leprosy treatment. Statins are among the most frequently prescribed drugs worldwide due to their beneficial effects on
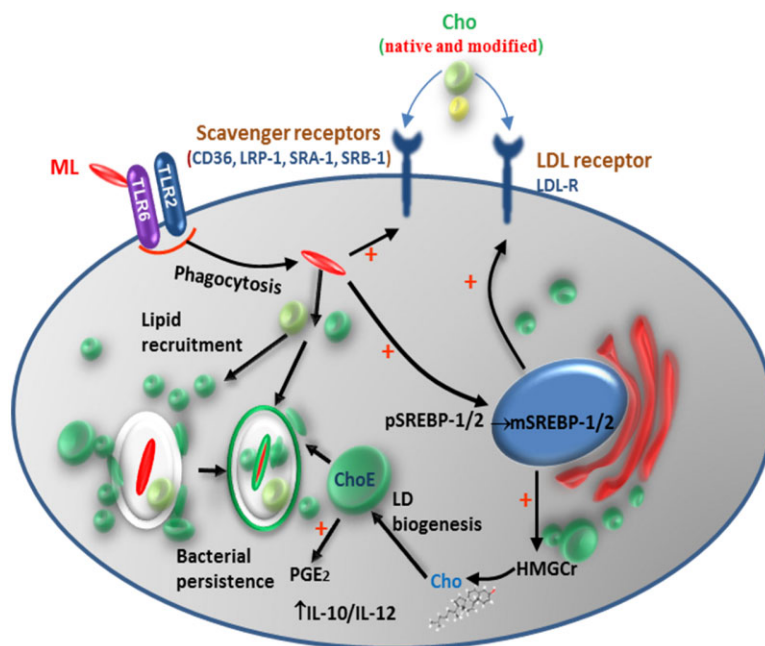
Fig. 9. A model for host cholesterol acquisition pathways by intracellular ML in macrophages. This figure depicts the potential sources of Cho for intracellular ML. ML infection stimulates the uptake of exogenous Cho sources (LDL) as well as the *de novo* synthesis of Cho via upregulation of the LDL receptor expression and the HMGCR enzyme, respectively, leading to LD formation. The modulation of Cho metabolism by ML involves the activation of the SREBP-1/2 transcription factors. Internalized LDL and LDs are recruited to bacterial-containing phagosomes where they accumulate. ML modulation of host cell lipid metabolism depends on the TLR2/TLR6 signalling cascade that elicits LD biogenesis and upregulation of CD36. LDs and exogenous lipid recruitment probably constitute an effective ML intracellular strategy to acquire host lipids as a nutritional source and promote bacterial survival. Moreover, accumulation of LDs in infected macrophages favours the generation of an innate immune response with PGE_2 production and a high IL-10/IL-12 ratio (Mattos *et al.*, 2010), which may contribute to a permissive environment for ML proliferation. LD: lipid droplet; ML: *M. leprae*; Cho, cholesterol; ChoE: cholesteryl ester; PGE_2: prostaglandin E_2; pSREBP: precursor SREBP; mSREBP: mature precursor.

cardiovascular disease. However, the positive effects of statins are known to go beyond their lipid-lowering attributes, which include anti-inflammatory and immuno-modulatory activities (Jain and Ridker, 2005; Blum and Shamburek, 2009). Recent reports have emphasized their ability to contribute to favourable outcomes of severe bacterial infectious diseases (Kopterides and Falagas, 2009). We have shown a direct bacterial killing effect of lovastatin linked to sterol pathway inhibition, reducing the levels of a major host lipid source to ML. Besides the direct microbicidal action on ML, the pleiotropic effects of statins could contribute to a better leprosy outcome by decreasing immunopathology and perhaps preventing the incidence of reactional episodes.

In conclusion, a model can be proposed in which the host lipid modulation phenomenon induced by ML plays a key role in leprosy pathogenesis by facilitating bacterial persistence in the host through two different mechanisms (Fig. 9). As indicated in our previous study, ML infection is able to induce the biogenesis of new LD organelles that constitute active catalytic sites of PGE_2, a potent immunomodulatory lipid mediator known to inhibit many

aspects of innate and adaptive immunity (Mattos *et al.*, 2010). Bacterial persistence results in part from the expression of an 'anti-inflammatory' phenotype dependent on lipid metabolism. Moreover, host lipids are modulated to form foam cells through ML-induced uptake, biosynthesis, and the subsequent recruitment of Cho to bacteria-containing phagosomes as an effective strategy to aid in ML survival. Cholesterol homeostasis dysregulation by ML is at least partially mediated by the induction and activation of transcriptional factors of the SREBPs family. The role of other transcriptional factors such as the nuclear receptor PPAR-γ in ML-induced host cell lipid modulation will be the focus of future investigation.

The data presented herein extend our knowledge about the mechanisms of leprosy disease and sustain the idea that lipid modulation has pathophysiological conse-quences for bacterial persistence in the host. In turn, this knowledge paves the way for the discovery of novel targets for pharmacological drugs that could control mycobacterial infection by acting either directly or indi-rectly on the host cell metabolic pathways that are critical for bacterial survival.

Experimental procedures

Ethics statement

For the use of human samples, written informed consent was obtained and the procedures described were approved by the Ethics Committee of the Oswaldo Cruz Foundation. Animal protocols were in agreement with the animal care guidelines of the National Institutes of Health and were approved by the Animal Welfare Committee of the Oswaldo Cruz Foundation (under permit number L-0002/08).

Antibodies

The following antibodies were used: guinea pig and mouse monoclonal against Adipose Differentiation Related Protein (ADRP; Research Diagnostics, Concord, MA, USA), monoclonal anti-α-tubulin (BD Transduction Laboratories, Franklin Lakes, NJ, USA), CS-35 anti-lipoarabinomannan (LAM) monoclonal, rabbit anti-whole ML (kindly provided by Dr Patrick J. Brennan, Colorado State University, Fort Collins, CO, USA; NIH/NIAID contract 1AI25469), anti-SR-A1 (mouse monoclonal, SC-166184), SREBP-1 (rabbit polyclonal, SC-8984), LDL-R (goat polyclonal, SC-11824), anti-HMGCR (SC-33827, rabbit polyclonal IgG) and anti-GADPH (mouse monoclonal) from Santa Cruz Biotechnology (Santa Cruz, CA, USA), anti-CD36 (rabbit polyclonal; Cayman Chemical, Ann Arbor, MI, USA) and anti-CD36 (rat monoclonal, Ab80080), SREBP-2 (rabbit polyclonal, ab30682) from Abcam (Cambridge, MA, USA), fluorescent-labelled (Alexa Fluor 488, 555, and 633) goat anti-rabbit and anti-mouse (Molecular Probes, Eugene, OR, USA), donkey anti-guinea pig fluorescent-dye-Cy2 conjugated, and, lastly, control IgG (Jackson ImmunoResearch Laboratories, West Grove, PA, USA).

Patients and skin biopsies

Six patients with lepromatous leprosy (LL) and four with borderline tuberculoid leprosy (BT) classified according to the Ridley and Jopling criteria were included in this study (Ridley and Jopling, 1966). All were in attendance at the Leprosy Outpatient Unit of the Oswaldo Cruz Foundation, Rio de Janeiro, RJ, Brazil. After informed consent, skin biopsy specimens (6 mm punch) were obtained before treatment and used for immunohistochemistry, mRNA expression, metabolite extraction, and isolation of macrophages.

Mycobacterium *species*

ML prepared from the footpads of athymic *nu/nu* mice was obtained from the National Hansen's Disease Program and the Instituto Lauro de Souza Lima (Bauru, São Paulo, Brazil). *M. bovis* BCG Pasteur (ATCC 35734) were grown as described (Mattos *et al.*, 2011b). Part of the isolated bacteria was killed by gamma-irradiation (1 MRad). This dose of irradiation was shown to inhibit both ML growth and metabolism (Adams *et al.*, 2000). Prior to some interactive assays, bacteria were pre-labelled using the PKH26 Red Fluorescence cell linker Kit (Sigma, St Louis, MO, USA), according to the manufacturer's instructions.

Animals

C57BL/6 (B6) mice along with TLR2 and TLR6 knockout mice on a homogeneous C57BL/B6 background were obtained from the Oswaldo Cruz Foundation breeding unit (Rio de Janeiro, RJ, Brazil).

Extraction of metabolites

For metabolite extraction, frozen biopsies obtained from the skin of BT and LL patients were thawed on ice, mechanically disrupted, extracted with chloroform, methanol and water (1:2:0.8 by vol) (Bligh and Dyer, 1959), and then partitioned with chloroform and methanol (2:1 by vol), according to the standard procedure of Folch *et al.* (1957). Pellets were extracted again with acetonitrile (10 µl of acetonitrile for each mg of initial tissue) by vortexing for 10 min. Samples were clarified by centrifugation at 16 000 *g* for 5 min, all phases were combined and extracts were dried for analysis through direct-infusion ultrahigh-resolution Fourier transform ion cyclotron resonance mass spectrometry (DI-FT-ICR MS). Alternatively, neutral lipids were extracted from leprosy skin biopsies and from ML-infected and uninfected cell cultures by the Folch procedure as described above and analysed by high performance, thin-layer chromatography (HPTLC).

DI-FT-ICR MS analysis

Dried extracts were resuspended in 60% acetonitrile (100 µl per 10 mg of sample), vortexed, sonicated, and cleared by centrifugation, as previously described (Antunes *et al.*, 2011; Amaral *et al.*, 2013). Extracts were diluted 1:3 in ESI standard solutions containing either 0.2% formic acid (positive ion mode) or 0.5% ammonium hydroxide (negative ion mode). Samples were then infused through a syringe pump (KDS Scientific, Holliston, USA) at a flow rate of 2.5 µl min^{-1} into a 12-T Apex-Qe hybrid FT-ICR mass spectrometer (Bruker Daltonics, Billerica, USA) equipped with an Apollo II electrospray ionization (ESI) source, a quadrupole mass filter, and a hexapole collision cell. Data were recorded in positive and negative ion modes with broadband mode detection and within *m/z* of 180–1000 Daltons for the positive mode and 180–1100 for the negative mode. Survey scan mass spectra in positive and negative ion modes were acquired from the accumulation of 400 scans per spectrum and duplicate acquisitions per sample.

Data processing

Raw mass spectrometry data were processed exactly as previously described (Antunes *et al.*, 2011). To identify differences in metabolite composition between BT and LL biopsy samples, we selected metabolites that were present in one set of samples but not in the other. We also averaged the intensities of the remaining masses in each group, calculated the ratios between averaged intensities, and compared the two groups. Metabolites showing at least twofold changes were selected for further analysis. To assign possible metabolite identities to the selected masses, the monoisotopic neutral masses of interest were queried against MassTrix (http://masstrix.org), a free-access software designed to incorporate masses into metabolic pathways using the Kyoto Encyclopedia of Genes and Genomes (KEGG; http://www

.genome.jp/kegg/). Masses were searched against the *Homo sapiens* database within a mass error of 3 ppm.

HPTLC analysis

Neutral lipids were analysed by one-dimensional HPTLC on Silica gel 60 plates (Merck, Darmstadt, Germany). Plates were first developed in hexane, ethyl ether, acetic acid (60:40:1 by vol) until the solvent front reached the middle of the plate and then in hexane, chloroform, acetic acid (80:20:1 by vol). HPTLC plates were stained by spraying with a charring solution consisting of 10% $CuSO_4$, 8% H_3PO_4, and heated to 180°C for 5–10 min (Ruiz and Ochoa, 1997). The charred HPTLC plate was then subjected to densitometric analysis using a photodensitometer with automatic peak integration (Camag TLC Scanner II). The percentage of each lipid class was calculated from the total amount of lipids (set as 100%) isolated from each skin biopsy.

Cell isolation from skin biopsies

Infected macrophages were isolated from LL biopsies using a modified protocol from that described by Moura *et al.* (2007). In summary, immediately after collection, the biopsies were placed in a tube with RPMI 1640 medium on ice. The epidermis was gently withdrawn with a razor blade; and the dermis was minced and incubated at 37°C with an enzyme mixture in RPMI medium with 10% of serum (0.5 mg ml^{-1} collagenase and 50 g ml^{-1} dispase). The cells were washed twice in phosphate-buffered saline (PBS) and plated in RPMI 1640 supplemented with 2 mM L-glutamine and 2% heat-inactivated fetal calf serum (FCS). After testing cell viability by trypan blue exclusion, 1×10^5 cells were added to 12 mm round glass coverslips in 24-well plates and incubated with 10% FCS at 33°C in a humid atmosphere with 5% CO_2 for 1 day.

Isolation and treatment of mononuclear phagocytes with ML

Buffy coats were obtained from normal donors (healthy controls, HC) at the Hemotherapy Service of the Clementino Fraga Filho University Hospital, associated with the Federal University of Rio de Janeiro, RJ, Brazil. The procedures described in this work were approved by the Ethics Committee of the Oswaldo Cruz Foundation. Human PBMCs were prepared by way of Ficoll-Hypaque density gradient centrifugation (Sigma Chemical), and monocytes were isolated and infected with ML with a moi of 5 as described (Mattos *et al.*, 2010), except for the dose–response experiments (moi of 2.5 and 5). Cultures were incubated for 48 h, except for viability studies (72 h) at 33°C. In some experiments, cells were infected with BCG (moi of 5 for 72 h) at 37°C. Mouse resident peritoneal macrophages were isolated from unstimulated mice and infected with ML as described (Mattos *et al.*, 2010).

RNA isolation, cDNA synthesis and real-time polymerase chain reaction

RNA was isolated from frozen samples as described (Moura *et al.*, 2012). cDNA was made from DNase-treated RNA using Superscript II (Invitrogen), and was then employed for qRT-PCR amplification using a StepOne Plus (Applied Biosystems) and Power SYBR Green PCR Master Mix (Applied Biosystems Made, UK). Gene expression analysis was performed using the primers displayed in Supplementary Table S1. Glyceraldehyde-3-phosphate dehydrogenase (GAPDH) was used as the standard housekeeping gene.

Flow cytometry analysis

Adherent cells were detached by trypsin-EDTA treatment (Invitrogen) and processed as described (Mattos *et al.*, 2010). Samples were incubated with primary antibodies (anti-CD36 or anti-IgG1 isotype control) and secondary antibody [monoclonal fluorescein isothiocyanate (FITC)]. The induction of this receptor was measured in the FL1 channel and was expressed as mean fluorescence intensity (MFI). Bacterial association to cells was measured at FL2 by observing PKH26-labelled bacteria. The index of bacterial association is expressed as the percentage of cells taking up PKH26-ML. Flow cytometric acquisition and analysis were performed on a FACSCalibur flow cytometer (BD Biosciences, Heidelberg, Germany), and at least 10 000 cells were analysed per sample. Quantitative data analysis was performed using BD CellQuest Pro software (BD Biosciences) and WinMDI analysis software.

Preparation of LDL

LDL was isolated from fresh human plasma as described (Poumay and Ronveaux-Dupal, 1985). The lipoprotein concentration was expressed in terms of protein content, as determined by the BCA Protein Assay Kit. The fluorescent lipid BODIPY-cholesterol (BODIPY-Cho) was incorporated into LDL by mixing 50 µl of the lipid stock solution with 20 ml of filtered fresh human plasma. After incubation for 16 h at 37°C, LDL was isolated as described (Hummon *et al.*, 2007).

Cellular uptake of LDL-cholesterol

The uptake of LDL-Cho by monocytic cells was determined by incubating the cells with unlabelled LDL-Cho, fluorescent LDL-[BODIPY-Cho] or radiolabelled LDL-[^{3}H]-Cho. Cells were treated with ML for 48 h being the cultures pulsed with 0.1 mg ml^{-1} unlabelled LDL-Cho or LDL-[BODIPY-Cho] during the last 2 h of incubation in serum-free medium. The unlabelled LDL-Cho uptake was determined by filipin staining and fluorometric enzymatic assay as described below. Cells pulsed with LDL-[BODIPY-Cho] were rinsed with PBS several times prior to the addition of a 0.05% trypsin solution. When a single-cell suspension was obtained, trypsin was neutralized using complete medium. After centrifugation, the cells were washed with PBS, fixed with 4% PFA, and rewashed with PBS. After the exclusion of cell debris by gating on characteristic forward and side scatter, 10 000 cells were measured in each sample. Fluorescence intensity of the cells with internalized fluorescent Cho conjugates was measured upon excitation at 488 nm and emission at 530 ± 30 nm at a constant intensity in all experiments. The geometric mean values were calculated as the magnitude of internalized fluorescence and plotted.

Alternatively, the activity of LDL-R was verified using radiolabelled LDL-[^{3}H]-Cho. Briefly, 1×10^6 cells per well infected or not as described above were incubated with 1×10^6 CPM of Cho-LDL-[^{3}H]-Cho in RPMI medium without serum for 6 h. Excess of radiolabelled LDL was washed, and the cells were detached using EDTA. Cell suspensions were subsequently analysed using a Beckman LS5801 counter (Beckman Instruments, High Wycombe, Buckinghamshire, UK).

Measurements of cholesterol content

The Cho content of cells was monitored by the intensity of fluorescence emissions from the polyene antibiotic filipin (Sigma). Adhering cells were detached using 0.05% trypsin solution, fixed in 4% PFA for 10 min, and washed with PBS. Cells were incubated with 0.1 mg ml^{-1} filipin in the presence of 0.1% saponin for 60 min, and the cellular Cho content was monitored by measuring the intensity of fluorescence emission from filipin at 325–510 nm by flow cytometry, as described above. For total Cho determination the Amplex Red Cholesterol Red Assay Kit (Molecular Probes) was used. Briefly, 4×10^5 cells per well infected or not as described above were lysated with radioimmunoprecipitation assay (RIPA) buffer. The lysates were centrifuged at 13 000 g for 10 min and Cho was measured in the supernatants using a fluorometer (585 nm) as described by the manufacturer.

Analysis of cholesterol biosynthesis

To study *de novo* Cho biosynthesis, macrophages were metabolically labelled with [^{3}H] acetate (10 µCi ml^{-1}, 0.1 mM) in RPMI-1640 medium containing 0.2% FCS and infected with live ML for 48 h. Cells were washed three times with 1 ml of ice-cold PBS before being scraped into 1 ml of PBS and sonicated for 10 s at 22 kHz to provide cell homogenates. Samples (0.5 ml) of cell homogenates were extracted by the Bligh and Dyer method (Bligh and Dyer, 1959). The organic phases were dried under a stream of N$_2$ and dissolved in 50 µl of chloroform containing 8 mg ml^{-1} of each lipid standard. Samples (40 µl) were applied to 20 cm silica HPTLC (Whatman, Maidstowe, UK) and developed for 18 cm in hexane, diethyl ether, glacial acetic acid (70:30:2 by vol). Lipid bands were detected with I$_2$ vapour and were scraped from the plate into 5 ml of Picofluor 40 scintillant (Packard, Groningen, The Netherlands). Radioactivity was determined by counting samples using a Beckman LS5801 counter (Beckman Instruments, High Wycombe, Buckinghamshire, UK).

Optical and fluorescence microscopy

Immunohistochemical procedures in skin biopsies were performed as described (Mattos *et al.*, 2011a). Briefly, tissue sections were thawed on pre-coated sylane slides and subjected to staining and immunostaining protocols. For immunocytochemical staining of macrophages isolated from LL biopsies and from human PBMC, cells seeded on coverslips were fixed in 4% PFA and processed as described (Mattos *et al.*, 2011a). Immunostaining was performed by incubation with primary antibodies to ADRP and ML (anti-whole bacteria or anti-LAM). Fluorescent secondary antibodies were incubated for 2 h at room temperature. To visualize fluorescent Cho, infected cells were labelled with 0.1 mg of LDL-[BODIPY-Cho] for 2 h. Coverslips

were washed to remove the excess of labelling, fixed with 4% PFA for 10 min, rewashed with PBS, and then mounted. Cytochemical staining of β-hydroxysterols with filipin (25 µg ml^{-1} of filipin for 15 min) or of LDs with BODIPY493/503 dye [1 µM BODIPY (4,4-difluoro-1,3,5,7,8-pentamethyl-4-bora-3a,4a-diaza-s-indacene, Molecular Probes) for 45 min] was processed and analysed by phase-contrast and fluorescence microscopy as described (Mattos *et al.*, 2011a). Nuclei were stained with TO-PRO-3 (Molecular Probes). Cells were mounted with the VectashieldHard set-mounting medium (Vector Laboratories). Confocal images were acquired using a LSM 510 Zeiss confocal microscope (Zeiss, Jena, Germany) and processed by LSM 510 Zeiss software. Alternatively, cells were directly observed with an epifluorescence microscope (Microphot FXA; Nikon). Images were captured with a CCD camera (Photometrics), processed with Image-Pro Plus (Media Cybernetics), and their contrast was enhanced with Adobe Photoshop 5.0 (Adobe Systems). Contrast images were acquired using differential interferential contrast (DIC).

To detect SR-A1 immunohistochemical labelling of cryostat sections (5 µm) was performed as described previously (de Souza Sales *et al.*, 2011). Sections were incubated with anti-SR-A1 (1:50) (D-8, Santa Cruz Biotechnology, Dallas, Texas, USA). The negative controls were performed by omitting the primary antibody, and no labelling was observed. The slides were examined on a Nikon E400 light microscope (Japan); and the images were captured via a video-microscopic system composed of a Nikon E400 microscope, CoolSNAP-Procf Color camera, and Infinity analysis software.

Tissue processing for TEM

Lepromatous leprosy skin biopsies were processed for TEM as described (Kaplan *et al.*, 1983). Briefly, biopsies were fixed in 2.5% glutaraldehyde in a 0.1 M cacodylate buffer containing 0.1 M sucrose (pH 7.4). The tissue was postfixed for 6 h at 4°C with 2% osmium tetroxide, stained *en bloc* in 0.25% uranyl acetate, dehydrated in a graded series of ethanol, and embedded in Epon. Thin sections were cut using a diamond knife on an ultramicrotome (Leica, Bannockburn, IL, USA). Sections were mounted on uncoated 200-mesh copper grids before staining with uranyl acetate and lead citrate and viewed with a transmission electron microscope (Tecnai Spirit G12, FEI, the Netherlands) at 60 KV. At least 75 electron micrographs randomly taken at different magnifications were analysed.

Western blot analysis

Cell lysates were prepared in reducing and denaturing conditions and subjected to electrophoresis in SDS-PAGE gels according to the molecular weight of the protein under investigation. Proteins from skin biopsies were obtained from archived samples following TRIZOL® isolation of RNA and DNA, as described by Hummon *et al.* (2007). Protein content was determined by the BCA™ Protein Assay Reagent kit (Pierce, Rockford, IL, USA) using serum albumin as a standard. Western blot was developed with anti-HMGCR antibody, anti-CD36, anti-SREBP-1 and anti-SREBP-2. α-tubulin or GADPH were used as loading controls. For densitometry analysis, the ECL images of the developed films were performed using the public domain ImageJ program

(developed at the National Institutes of Health and available at http://rsb.info.nih.gov/ij/), using the 'Gel Analysis' functions.

Mycobacterium *viability*

A live/dead staining protocol based on the LIVE/DEAD Bactlight Bacterial viability Kit (Invitrogen) was applied to estimate the viable versus non-viable ML and BCG obtained from macrophages in several conditions of Cho privation. In brief, macrophages (2×10^6 cells per well) were infected with ML (moi 5:1), incubated for 2 h at 33°C, and then washed with PBS (3×) to remove any uninternalized bacteria. The infected cultures were then incubated in RPMI medium supplemented with 2% FCS or in the fully defined serum-free AIM V medium (Gibco BRL) in the presence or absence of lovastatin (1 μM, Sigma-Aldrich, St. Louis, MO, USA). Alternatively, BCG-infected macrophages (moi 5:1) were incubated in RPMI supplemented with 2% FCS or with delipidated serum (2% dLDL). Cultures were treated with lovastatin or vehicle in RPMI medium. In parallel, Cho (1 μM, Sigma) and ergosterol (1 μM, Sigma) supplementation was used as a lipid source in medium supplemented with delipidated serum. Cultures were incubated for 72 h at 33°C. Afterwards, cells were lysed with 0.1% saponin and bacteria were labelled with the LIVE/DEAD kit. The percentages of live/dead bacteria were determined by flow cytometry according to the manufacturer's instructions. As controls, bacterial suspensions were exposed to lovastatin or DMSO (Sigma) using the conditions described above to exclude the direct drug effect on bacterial metabolism. Flow cytometry measurements were performed on a FACSCalibur (BD Bioscience) and analysed via CellQuest software (BD Bioscience). The MTT [3-(4,5-dimethylthiazol-2-yl)-2,5-diphenyltetrazolium bromide, Sigma] assay was used to measure cellular toxicity in response to the drug treatments (Mosmann, 1983).

Statistical analysis

Data analysis was performed using the GraphPad InStat program (GraphPad Software, San Diego, CA, USA), and the statistical significance $P \leq 0.05$) was determined by Student's *t*-tests.

References

Adams, L.B., Soileau, N.A., Battista, J.R., and Krahenbuhl, J.L. (2000) Inhibition of metabolism and growth of *Mycobacterium leprae* by gamma irradiation. *Int J Lepr Other Mycobact Dis* **68:** 1–10.

Almeida, P.E., Silva, A.R., Maya-Monteiro, C.M., Töröcsik, D., D'Avila, H., Dezsö, B., *et al.* (2009) *Mycobacterium bovis* bacillus Calmette-Guérin infection induces TLR2-dependent peroxisome proliferator-activated receptor gamma expression and activation: functions in inflammation, lipid metabolism, and pathogenesis. *J Immunol* **183:** 1337–1345.

Almeida, P.E., Roque, N.R., Magalhães, K.G., Mattos, K.A., Teixeira, L., Maya-Monteiro, C., *et al.* (2014) Differential TLR2 downstream signaling regulates lipid metabolism and cytokine production triggered by *Mycobacterium bovis* BCG infection. *Biochim Biophys Acta* **1841:** 97–107.

Amaral, J.J., Antunes, L.C.M., de Macedo, C.S., Mattos, K.A., Han, J., Pan, J., *et al.* (2013) Metabonomics reveals drastic changes in anti-inflammatory/pro-resolving polyunsaturated fatty acids-derived lipid mediators in leprosy disease. *PLoS Negl Trop Dis* **7:** e2381. doi:10.1371/journal.pntd.0002381.

Antunes, L.C., Han, J., Ferreira, R.B., Lolić, P., Borchers, C.H., and Finlay, B.B. (2011) Effect of antibiotic treatment on the intestinal metabolome. *Antimicrob Agents Chemother* **55:** 1494–1503.

Av-Gay, Y., and Sobouti, R. (2000) Cholesterol is accumulated by mycobacteria but its degradation is limited to non-pathogenic fast-growing mycobacteria. *Can J Microbiol* **46:** 826–831.

Aviram, M., Keidar, S., and Brook, G.J. (1991) Dual effect of lovastatin and simvastatin on LDL-macrophage interaction. *Eur J Clin Chem Clin Biochem* **29:** 657–664.

Bligh, E.G., and Dyer, W.J. (1959) A rapid method of total lipid extraction and purification. *Can J Biochem Physiol* **37:** 911–917.

Blum, A., and Shamburek, R. (2009) The pleiotropic effects of statins on endothelial function, vascular inflammation, immunomodulation and thrombogenesis. *Atherosclerosis* **203:** 325–330.

Bozza, P.T., Magalhães, K.G., and Weller, P.F. (2009) Leukocyte lipid bodies – biogenesis and functions in inflammation. *Biochim Biophys Acta* **1791:** 540–551.

Brennan, P. (1984) *Mycobacterium leprae* – the outer lipoidal surface. *J Biosci* 685–689.

Brzostek, A., Pawelczyk, J., Rumijowska-Galewicz, A., Dziadek, B., and Dziadek, J. (2009) *Mycobacterium tuberculosis* is able to accumulate and utilize cholesterol. *J Bacteriol* **191:** 6584–6591.

Chatterjee, K.R., Das Gupta, N.N., and De, M.L. (1959) Electron microscopic observations on the morphology of *Mycobacterium leprae*. *Exp Cell Res* **18:** 521–527.

Cruz, D., Watson, A.D., Miller, C.S., Montoya, D., Ochoa, M.T., Sieling, P.A., *et al.* (2008) Host-derived oxidized phospholipids and HDL regulate innate immunity in human leprosy. *J Clin Invest* **118:** 2917–2928.

D'Avila, H., Melo, R.C., Parreira, G.G., Werneck-Barroso, E., Castro-Faria-Neto, H.C., and Bozza, P.T. (2006) *Mycobacterium bovis* bacillus Calmette-Guérin induces TLR2-mediated formation of lipid bodies: intracellular domains

for eicosanoid synthesis *in vivo*. *J Immunol* **176:** 3087–3097.

D'Avila, H., Maya-Monteiro, C.M., and Bozza, P.T. (2008) Lipid bodies in innate immune response to bacterial and parasite infections. *Int Immunopharmacol* **8:** 1308–1315.

Degang, Y., Akama, T., Hara, T., Tanigawa, K., Ishido, Y., Gidoh, M., *et al.* (2012) Clofazimine modulates the expression of lipid metabolism proteins in *Mycobacterium leprae*-infected macrophages. *PLoS Negl Trop Dis* **6:** e1936.

Elamin, A.A., Stehr, M., and Singh, M. (2012) Lipid droplets and *Mycobacterium leprae* infection. *J Pathog* **2012:** 361374.

Espenshade, P.J. (2006) SREBPs: sterol-regulated transcription factors. *J Cell Sci* **119:** 973–976.

Folch, J., Lees, M., and Sloane Stanley, G.H. (1957) A simple method for the isolation and purification of total lipides from animal tissues. *J Biol Chem* **226:** 497–509.

Goldstein, J.L., DeBose-Boyd, R.A., and Brown, M.S. (2006) Protein sensors for membrane sterols. *Cell* **24:** 35–46.

Hummon, A., Lim, S.R., Difilippantonio, M.J., and Ried, T. (2007) Isolation and solubilization of proteins after TRIZOL® extraction of RNA and DNA from patient material following prolonged storage. *Biotechniques* **42:** 467–472.

Jain, M.K., and Ridker, P.M. (2005) Anti-inflammatory effects of statins: clinical evidence and basic mechanisms. *Nat Rev Drug Discov* **4:** 977–987.

Jeon, T., I, and Osborne, T.O. (2012) SREBPs: metabolic integrators in physiology and metabolism. *Trends Endocrinol Metab* **23:** 65–72.

Kaplan, G., Van Voorhis, W.C., Sarno, E.N., Nogueira, N., and Cohn, Z.A. (1983) The cutaneous infiltrates of leprosy. A transmission electron microscopy study. *J Exp Med* **158:** 1145–1159.

Kim, M.J., Wainwright, H.C., Locketz, M., Bekker, L.G., Walther, G.B., Dittrich, C., *et al.* (2010) Caseation of human tuberculosis granulomas correlates with elevated host lipid metabolism. *EMBO Mol Med* **2:** 258–274.

Kopterides, P., and Falagas, M.E. (2009) Statins for sepsis: a critical and updated review. *Clin Microbiol Infect* **15:** 325–334.

Lee, W., VanderVen, B.C., Fahey, R.J., and Russell, D.G. (2013) Intracellular *Mycobacterium tuberculosis* exploits host-derived fatty acids to limit metabolic stress. *J Biol Chem* **288:** 6788–6800.

Mattos, K.A., D'Avila, H., Rodrigues, L.S., Oliveira, V.G., Sarno, E.N., Atella, G.C., *et al.* (2010) Lipid droplet formation in leprosy: Toll-like receptor-regulated organelles involved in eicosanoid formation and *Mycobacterium leprae* pathogenesis. *J Leukoc Biol* **87:** 371–384.

Mattos, K.A., Lara, F.A., Oliveira, V.G., Rodrigues, L.S., D'Avila, H., Melo, R.C., *et al.* (2011a) Modulation of lipid droplets by *Mycobacterium leprae* in Schwann cells: a putative mechanism for host lipid acquisition and bacterial survival in phagosomes. *Cell Microbiol* **13:** 259–273.

Mattos, K.A., Oliveira, V.G., D'Avila, H., Rodrigues, L.S., Pinheiro, R.O., Sarno, E.N., *et al.* (2011b) TLR6-driven lipid droplets in *Mycobacterium leprae*-infected Schwann cells: immunoinflammatory platforms associated with bacterial persistence. *J Immunol* **187:** 2548–2558.

de Mattos, K.A., Sarno, E.N., Pessolani, M.C., and Bozza, P.T. (2012) Deciphering the contribution of lipid droplets in leprosy: multifunctional organelles with roles in *Mycobacterium leprae* pathogenesis. *Mem Inst Oswaldo Cruz* **107** (Suppl. 1)**:** 156–166.

van der Meer-Janssen, Y.P., van Galen, J., Batenburg, J.J., and Helms, J.B. (2010) Lipids in host–pathogen interactions: pathogens exploit the complexity of the host cell lipidome. *Prog Lipid Res* **49:** 1–26.

Montoya, D., Cruz, D., Teles, R.M., Lee, D.J., Ochoa, M.T., Krutzik, S.R., *et al.* (2009) Divergence of macrophage phagocytic and antimicrobial programs in leprosy. *Cell Host Microbe* **6:** 343–353.

Mosmann, T. (1983) Rapid colorimetric assay for cellular growth and survival: application to proliferation and cytotoxicity assays. *J Immunol Methods* **65:** 55–63.

Moura, D.F., Teles, R.M., Ribeiro-Carvalho, M.M., Teles, R.B., Santos, I.M., Ferreira, H., *et al.* (2007) Long-term culture of multibacillary leprosy macrophages isolated from skin lesions: a new model to study *Mycobacterium leprae*-human cell interaction. *Br J Dermatol* **157:** 273–283.

Moura, D.F., de Mattos, K.A., Amadeu, T.P., Andrade, P.R., Sales, J.S., Schmitz, V., *et al.* (2012) CD163 favors *Mycobacterium leprae* survival and persistence by promoting anti-inflammatory pathways in lepromatous macrophages. *Eur J Immunol* **42:** 2925–2936.

Pandey, A.K., and Sassetti, C.M. (2008) Mycobacterial persistence requires the utilization of host cholesterol. *Proc Natl Acad Sci USA* **105:** 4376–4380.

Parihar, S.P., Guler, R., Khutlang, R., Lang, D.M., Hurdayal, R., Mhlanga, M.M., *et al.* (2014) Statin therapy reduces the *Mycobacterium tuberculosis* burden in human macrophages and in mice by enhancing autophagy and phagosome maturation. *J Infect Dis* **209:** 754–763.

Peyron, P., Vaubourgeix, J., Poquet, Y., Levillain, F., Botanch, C., Bardou, F., *et al.* (2008) Foamy macrophages from tuberculous patients' granulomas constitute a nutrient-rich reservoir for *M. tuberculosis* persistence. *PLoS Pathog* **4:** e1000204.

Poumay, Y., and Ronveaux-Dupal, M.F. (1985) Rapid preparative isolation of concentrated low density lipoproteins and of lipoprotein-deficient serum using vertical rotor gradient ultracentrifugation. *J Lipid Res* **26:** 1476–1480.

Prasad, P.V., and Kaviarasan, P.K. (2010) Leprosy therapy, past and present: can we hope to eliminate it? *Indian J Dermatol* **55:** 316–324.

Reiss, A.B., and Glass, A.D. (2006) Atherosclerosis: immune and inflammatory aspects. *J Investig Med* **54:** 123–131.

Ridley, D.S., and Jopling, W.H. (1966) Classification of leprosy according to immunity. A five-group system. *Int J Lepr Other Mycobact Dis* **34:** 255–273.

Ruiz, J.I., and Ochoa, B. (1997) Quantification in the subnanomolar range of phospholipids and neutral lipids by monodimensional thin-layer chromatography and image analysis. *J Lipid Res* **38:** 1482–1489.

Saka, H.A., and Valdivia, R. (2012) Emerging roles for lipid

droplets in immunity and host–pathogen interactions. *Annu Rev Cell Dev Biol* **28:** 411–437.

Sakurai, I., and Skinsnes, O.K. (1970) Lipids in leprosy. 2. Histochemistry of lipids in human leprosy. *Int J Lepr Other Mycobact Dis* **38:** 389–403.

Scollard, D.M., Adams, L.B., Gillis, T.P., Krahenbuhl, J.L., Truman, R.W., and Williams, D.L. (2006) The continuing challenges of leprosy. *Clin Microbiol Rev* **19:** 338–381.

Singh, V., Jamwal, S., Jain, R., Verma, P., Gokhale, R., and Rao, K.V. (2012) *Mycobacterium tuberculosis*-driven targeted recalibration of macrophage lipid homeostasis promotes the foamy phenotype. *Cell Host Microbe* **12:** 669–681.

de Souza Sales, J., Lara, F.A., Amadeu, T.P., de Oliveira Fulco, T., da Costa Nery, J.A., Sampaio, E., *et al.* (2011) The role of indoleamine 2, 3-dioxygenase in lepromatous leprosy immunosuppression. *Clin Exp Immunol* **165:** 251–263.

Tanigawa, K., Suzuki, K., Nakamura, K., Akama, T., Kawashima, A., Wu, H., *et al.* (2008) Expression of adipose differentiation-related protein (ADRP) and perilipin in macrophages infected with *Mycobacterium leprae*. *FEMS Microbiol Lett* **289:** 72–79.

Tanigawa, K., Degang, Y., Kawashima, A., Akama, T., Yoshihara, A., Ishido, Y., *et al.* (2012) Essential role of hormone-sensitive lipase (HSL) in the maintenance of lipid storage in *Mycobacterium leprae*-infected macrophages. *Microb Pathog* **52:** 285–291.

Virchow, R. (1863) *Die krankhaften Geschwülste*. August Hirschwald. Berlin, Germany. 208.

Wenk, M.R. (2006) Lipidomics of host–pathogen interactions. *FEBS Lett* **580:** 5541–5551.

WHO (2011) Leprosy Today. WHO Report [WWW document]. URL http://www.who.int/lep/en/.

van der Wulp, M.Y., Verkade, H.J., and Groen, A.K. (2013) Regulation of cholesterol homeostasis. *Mol Cell Endocrinol* **368:** 1–16.

Supporting information

Additional Supporting Information may be found in the online version of this article at the publisher's web-site:

Fig. S1. ML induces total cholesterol content in human monocyte. Total Cho was quantified in cells treated or not with live and dead ML after incubation for 48 h. Cho levels were determined by Amplex Red Cholesterol Kit and normalized to total protein.

Fig. S2. Immunofluorescence staining control in LL biopsy and Virchow's cell. (A) LL biopsies and (B) Virchow's cells were either double-stained with specific isotype-matched control antibody or labelled with secondary antibody (red and green) and no fluorescence was observed.

Fig. S3. A simplified flow chart showing the experimental strategy employed to determine the importance of exogenous and endogenous cholesterol sources on mycobacterial viability.

Fig. S4. Effect of lovastatin on LDL-macrophage uptake. Monocytes infected or not with ML were incubated with LDL-[BODIPY-Cho] in the presence or not of lovastatin. The uptake of this exogenous Cho source was determined by flow cytometry in the FL1 channel and the internalized MFI values of [BODIPY-Cho]-LDL are expressed in bar graphs and represent an estimated level of LDL-Cho uptake. Statistically significant ($P \le 0.05$) differences are indicated by asterisks.

Fig. S5. Intracellular BCG viability and its correlation with cholesterol host metabolism. Macrophages were treated or not with statin and depleted of LDL from serum (dLDL or serum-free) or not (supplemented with FCS) to determine the role of Cho pathways in mycobacterial survival. The percentage of live and dead bacteria was evaluated using the LIVE/DEAD BacLight Bacterial Viability Kit in combination with flow cytometry after 72 h of drug treatment. FCS: fetal calf serum; dLDL: LDL-delipidated serum; Lov: lovastatin; Cho: free cholesterol; Erg: ergosterol; DMSO: control. Statistically significant ($P \le 0.05$) differences are indicated by asterisks.

Table S1. Sequences of primers used in this study.